EUROPEAN ORGANIZATION FOR NUCLEAR RESEARCH

CERN-EP/80-74
23 May 1980

HIGH FLUX OPERATION OF THE GATED MULTISTEP AVALANCHE CHAMBER

A. Breskin[×], G. Charpak, S. Majewski[+], G. Melchart, A. Peisert and F. Sauli

CERN, Geneva, Switzerland

F. Mathy

CEN, Saclay, France

and

G. Petersen

Niels Bohr Institute, Copenhagen, Denmark

ABSTRACT

A multiple gaseous detector based on the preamplification and transfer mechanism has been tested in a high radiation flux environment. The device, named gated multistep avalanche chamber, can detect and localize with good space and time accuracies selected tracks in minimum ionizing particle fluxes exceeding 10^5 s^{-1} mm^{-2}. The general operation properties, as well as some of the problems encountered are discussed.

Submitted to Nuclear Instruments and Methods

×) Present address: The Weizmann Institute of Sciences, Rehovoth, Israel.

+) Present address: Institute of Experimental Physics, Warsaw University, Poland.

1. INTRODUCTION

The original motivation for the development of the multistep avalanche chamber has been an attempt to overcome the limited flux capability of the multiwire proportional chamber (MWPC), caused by the space charge effects of positive ions[1]. The idea was to realize a composite structure in which the over-all gas proportional gain M, needed for detection of minimum ionizing particles, could be obtained as a product of two independent amplification elements of effective gain M_1 and M_2, respectively. Under control of an electronic shutter or gate, however, only selected events could receive the full gain $M_1M_2 = M$. The number of positive ions produced per unit time in the second amplifying element at a particle flux R is then:

$$nRM_2(1 + fM_1) \ , \tag{1}$$

where n is the number of primary charges liberated in the drift space of the two amplifying elements by the ionizing particle (assumed for simplicity to be the same in the two detection elements) and f the ratio between selected and total particle flux. Obviously, for $f \ll 1$, the reduction of positive charges in the second element equals M_1, as compared with a normal counter having gain M. For an over-all gain of around 10^5, suitable for minimum ionizing particle detection, and assuming $M_1 \simeq M_2$, a positive space-charge reduction by a factor of 100 is realized at a triggering rate f of 1%. Following Hendricks[2], the gain reduction in a proportional counter at a flux R depends exponentially on the total number of ions produced; in the quoted example, one should therefore, in principle, increase the flux capability of a gated chamber by two orders of magnitude. At high rates the device can be used, of course, only for track sampling, either random or under a triggering condition imposed by accessory equipment.

The practical realization of the proposed structure depends entirely on the possibility of implementing a region of gaseous amplification with the transfer of a sizeable fraction of the electron avalanches to the following sections. Much work has been devoted to the understanding of the preamplification and transfer mechanism[3-5], and has led to a new family of gaseous detectors with peculiar

properties, finding applications already in ring imaging of Čerenkov photons[6-8] and radio-chromatography imaging[9]. The present paper presents the preliminary results obtained in the operation of a gated multistep avalanche chamber (GMSC), in the detection of minimum ionizing particles both at low and high fluxes.

2. PRINCIPLES OF CONSTRUCTION AND OPERATION

We have built a GMSC around an existing 100 × 100 mm^2 active area mechanical framework, although as we will see later, only a small fraction of the chamber (about 20 × 10 mm^2) was activated for the high rate beam measurements. The structure of the GMSC used is shown in fig. 1. The electrode identified by HV1 consists of a 10 μm thick aluminium foil, while electrodes HV2, HV3, and GND are implemented with stainless steel crossed wire grids, of 50 μm wire diameter and 500 μm pitch. The gate electrode and the read-out electrode (HV6) are two meshes of copper-beryllium 50 μm diameter wires, 500 μm apart and perpendicular to each other. The wires in the gate electrode are connected alternately to two independent high-voltage supplies, HV4 and HV5, and a pulsed operation of the gate can be obtained through a pair of capacitors as shown. The wire grid between the gate and the read-out electrode is grounded all around the chamber edges on a large copperized plate, and the quality of this grounding appears to be the major element in limiting capacitive pick-up of the gating pulse (several hundred volts) by the amplifier on the read-out electrode. For the same purpose, a symmetric bipolar gate pulsing was preferred to a simpler unipolar pulsing; indeed, a capacitive pick-up almost two orders of magnitude smaller than in a previously described chamber[4] was obtained.

The structure shown contains as gaseous amplifying elements two parallel-plate avalanche chambers, where high electric fields are required for electron multiplication (around 7 kV cm^{-1}). Spontaneous breakdown at the gap edges has to be avoided in order to attain a good working condition; we have found that in most cases a single thin insulating strip (mylar or Kapton, 50 to 100 μm thick and a few mm wide) extending in the gap at the edges between anode and cathode is sufficient to prevent edge breakdown. A good quality of the insulating frame

surface, machined fibre glass in our case, appears to be essential for a correct behaviour. The best way to avoid this kind of breakdown is however a physical increase in the gap thickness at the edges; methods to implement such a structure have been developed and will be described in a more specialized paper[10].

With a proper choice of the grids' potential, to be detailed in the following sections, electrons produced in the conversion space of the GMSC by an ionizing radiation can be preamplified and transferred into the first drift space. An identical value for the potentials of the alternate sets of wires in the gate, either d.c. (HV4 = HV5) or pulsed as shown in fig. 1 allows then the transfer of electrons to the drift region 2 and to the second step of amplification for selected events. Simple field inversion in the conversion region ($|HV1| < |HV2|$) allows also to operate the first section as a parallel-plate counter; despite the obvious disadvantage of such a configuration, i.e. a gain dependent on the position of the primary pair production within the gap, we have found that better time resolutions can thus be obtained, as will be described later in the "conversion off" condition. Localization was performed analysing the pulse-height distribution on the last set of wires, after suitable amplification and analogue-to-digital conversion. Details of the amplifiers and analogue-to-digital converters (ADCs) will not be given here, as they were identical to the MWPC cathode read-out system already described[11,12] except for the polarity of the detected signals; the typical charge amplifier's sensitivity was about 1 V/pC, with an output noise around 5 mV r.m.s.

A small on-line computer was used for the data storage and retrieval during the beam tests. The gas mixture for all the described measurements was argon-acetone in a 98-2 volume concentration.

For the beam tests, the GMSC was installed between two scintillation counters providing in coincidence the time reference for the generation of the gating pulse, at a rate conveniently reduced by a preset electronics paralysis. Also, for a survey of the localization properties of the device, we have installed in the line a conventional MWPC having 2.54 mm wire spacing and used in the drift mode, i.e.

recording the time of detection as referred to the trigger in a time-to-digital converter. Owing to the small beam spot size, about 10 mm^2, only two wires of the MWPC were illuminated, and this resulted in a very severe rate limitation due to space-charge build-up: indeed, the localization accuracy of the GMSC could only be measured at low particle fluxes (below 10^3 s^{-1} mm^{-2}, see section 6).

3. THE GATING FUNCTION

Figure 2 shows the absolute gain as a function of electric field measured in a 5 mm thick parallel-plate structure, identical to the two amplification elements of the GMSC. As discussed in detail in ref. 4, preamplification factors in excess of 10^4 can be obtained at fields around 7 kV/cm, with a subsequent transfer of part of the electron avalanche in the lower field region; the transfer efficiency is, in first approximation, equal to the fields' ratio. On the other hand, the gating function requires the generation of an electric field between the alternate wires sufficiently large to defeat the existing one, i.e. a difference of potential increasing with the value of the transfer field, the obvious limit being spontaneous breakdown between adjacent wires. We have found good operational conditions setting the transfer field in both drift regions around 1.3 kV/cm; as shown in Fig. 3, a full blocking of electrons' transfer through the gate is then obtained at a difference of potential between alternate wires $V_G = |HV4 - HV5| \simeq 180$ V. The average gate potential $\frac{1}{2}(HV4 + HV5)$ can instead be varied in a large range without modifying the over-all gate transparency (Fig. 4); indeed, losses of transmission from one region appear to be compensated by gains in the transfer to the next. Detailed measurements of electrons' grid transparency were given in ref. 4. In all measurements to be described we have adopted the following setting of the potentials: HV3 = -2 kV, $\frac{1}{2}(HV4 + HV5) = -0.7$ kV. The condition HV4 = HV5 = -0.7 kV corresponds then to a d.c. open gate, while full d.c. gate blocking is obtained at $|HV4 - HV5| = 200$ V.

In the d.c. blocked condition, the gate transparency can be restored by the application of a symmetric bipolar pulse of a total amplitude approaching the existing d.c. offset. Figure 5 shows the simple avalanche transition circuit

used to generate the gating pulses*); a cable shaping is used to adjust the length of the gate and two symmetric pulses are obtained through a pair of circuits with identical and inverted transformers. The identity of the symmetric pulses' shape and that of the loads is, as mentioned, one of the pick-up reducing factors; fig. 6 shows examples of the gating pulses for 60 ns and 30 ns shaping lengths, respectively. A 20 × attenuation probe was used to realize the pictures on the oscilloscope, the actual peak voltages at the chamber being ±100 V as required to counterbalance the d.c. offset. Rise- and fall-times of the pulses are purposely rather slow to reduce pick-up.

Under pulsed operation, the gate transmission depends on the gating pulse length when this is too short to let the full electron avalanche through. As will be documented in a subsequent paper[13], the longitudinal avalanche extension in the described conditions has a standard deviation of about 300 μm; with a typical value of electron drift-time around 20 ns mm^{-1}, one expects to start losing transmission for gate lengths below 20-30 ns. This is indeed the case, as shown in fig. 7. The pulsed gate transparency was measured irradiating the GMSC with a ^{55}Fe 5.9 keV X-ray source, at sufficiently high preamplification (around 10^4) so as to be able to detect the preamplified pulse directly on electrode HV3; the discriminated signal could then be used to trigger the gate generator at the proper time. The ratio of the observed pulse height on the last electrode HV6 under gating conditions, to the one measured at d.c. open gate determines the transmission. As apparent from the figure, a 30 ns FWHM gate is sufficient to guarantee full transmission of the drifting electron cloud.

The picture in fig. 8a shows the signals detected on the first preamplification electrode (upper trace, 5 mV/division) and on the second amplification gap under pulsed gate transmission (lower trace, 500 mV/division). As there is not enough screening between the gate and the preamplification electrode, a large pick-up swing is observed there at the time of pulsing; the coupling to the main amplification grid instead is visible only at a much increased scope sensitivity

*) Developed at CERN by J.C. Santiard and M. Kudła.

(fig. 8b, 5 mV/division). Notice also that, owing to the drift-time of the electrons from the gate to the avalanche amplification detection, around 200 ns, the residual pick-up is well separated in time from the physical signal and constitutes no problem in the detection.

4. RATE-DEPENDENT PHENOMENA

Using the beam of a collimated 8 keV X-ray generator we could increase the ionizing radiation flux to values largely in excess of the ones considered at the limit for correct MWPC operation [around 10^4 s^{-1} mm^{-2} [14])]. No decrease in the average pulse height was observed in the gated operation, thus confirming the validity of the starting assumptions. However, an unexpected problem appeared, which may set an ultimate limit to the rate capability of the multistep chamber: sudden gas breakdown in the region of the irradiation, intervening at gas gains which are lower the higher the flux. It is suspected that the cause of the rate-dependent breakdown around the source position is the local field increase induced by positive ions' space charge at the cathode surface. The practical implication of the observation is a limit on the maximum safe operational voltage, and therefore on the gas gain, for a given flux. Obtaining a full detection efficiency depends then on the capability of the wire electronics to discriminate properly between the charge signals at a chamber's gain below the critical one.

It is observed that in a multistep device, breakdown occurs always in the section with the higher charge densities, i.e. the last one for similar elements' gain. In fig. 9 the breakdown voltage in the second element, V_2, is shown as a function of the radiation flux (8 keV X-rays detected in the conversion region) both in the d.c. open gate condition and in the pulsed gate operation. The measurement bars in the second case correspond to two gate opening frequencies, given as a percentage of the total rate [the factor f in expression (1)]. Clearly, in the gated operation at high fluxes the operational voltage in the second amplification element can be higher by more than 500 V than in the d.c. open condition, corresponding to a gain factor of almost two orders of magnitude (see fig. 2). Notice

also that the breakdown voltage depends very little on the gate opening ratio; at low fluxes indeed, where it was possible to approach a 100% ratio (the limit being set by the recovery time, about 100 μs, of the avalanche transistor circuit), the working voltage in the pulsed operation is still about 300 V higher than in the d.c. open mode. Since in this case most of the converted X-rays are receiving the full amplification, the observation strongly suggests that the responsibility for the breakdown goes to a secondary extraction mechanism at the first cathode induced by positive ions. In the gated operation indeed the ions generated in the second element of amplification cannot reach the first, since generally they find the gate closed in their backward drift (even if the gate would randomly open at the proper time, its length of around 30 ns only lets through a minor fraction of the slowly migrating ions).

A systematic investigation of this phenomenon is under way, and its results will be published later[13]; in what follows, we will just consider the rate-dependent breakdown as a phenomenological limitation to the working voltage of the device.

5. HIGH FLUX BEAM MEASUREMENTS

The GMSC has been installed and operated at CERN in a high-intensity minimum ionizing charged particle beam, having an average surface at the detector position of about 10 mm^2. Because of intrinsic limitations in the rate capability of the pair of scintillation counters used for beam monitoring, a maximum intensity of about 10^7 counts/2 s spill was used, providing an average flux in the detector of 2×10^5 s^{-1} mm^{-2} (assuming a uniform illumination over a surface of 25 mm^2; as will be shown in the following, see for example fig. 24, this is a rather optimistic assumption). The beam trigger itself was provided by the coincidence of the two scintillation counters, one of which had a surface (16 mm^2) barely exceeding the beam spot size. The gating frequency was reduced to the maximum repetition rate allowed by the avalanche circuit, about 10^4 s^{-1}, by a 100 μs paralysis in the main coincidence. Owing to the small beam size, and in order to reduce the pick-up and noise problems, only a 20 mm wide strip in the gate electrode was

pulsed open, while all the surface of the gate (100 × 100 mm^2) was d.c. polarized. All detectors' efficiency measurements were then realized electronically using the logic sum of the discriminated output of twenty adjacent wires in the last amplification element; the average discrimination threshold on each wire had a value of 0.05 pC, corresponding to a 50 mV discrimination level at the output of the preamplifier having 1 V/pC sensitivity.

As already mentioned, the statistical fluctuations in the primary ion pairs' production tend to increase the avalanche size in the case of detection of charged particles, as compared with X-ray detection. This is apparent from fig. 10, showing the measured efficiency plateau in the described conditions and at moderate beam flux, both for a d.c. open gate and for the operation at several pulsed gate widths. The efficiency is given for constant preamplification and transfer voltages as a function of the second amplification voltage; setting $|HV1| > |HV2|$ (see fig. 1) includes in the detection the ionization produced in the upper region (conversion on), while $|HV1| < |HV2|$ defines the conversion off condition. The last mode of operation, as we will see in more detail, results in better time resolution and reduced memory for the detector, but has the obvious disadvantage of requiring higher chamber gains to detect the few electrons produced close to the upper surface of the preamplification region and receiving therefore full amplification. In our operating conditions, indeed, the average distance between primary ion pairs, 300 μm, is comparable with the mean distance of multiplication in the gap, about 500 μm for a gain of 10^4. Charges created within the preamplification volume receive therefore an exponentially decreasing multiplication for an increasing distance from the upper cathode. As a result the efficiency plateau is reached with difficulty, especially for short gate lengths; the maximum measured efficiency in the conversion off condition is indeed 98%, while it approches 99.5% in the conversion on operation. The difference in the detected charge profile for the two conditions is apparent from the pulse-height spectra shown in figs. 11a and b (conversion on and off, respectively). Notice that the second spectrum was measured at a much higher chamber gain than the first; the

bad detection statistics, corresponding essentially to the amplification of single electrons produced at variable depths in the gap, is apparent.

Since the avalanche propagation time is slightly decreasing with an increasing chamber gain, the pulsed gate timing has to be adjusted at each value of gain to reach full efficiency. Typical gate delay curves in the conversion off case are shown in fig. 12, for several values of V_2; the width of the coincidence reflects the width of the avalanche at a given discrimination level, and determines the memory of the detector, i.e. the chance to detect uncorrelated tracks at high fluxes. At the highest value of V_2, where full efficiency is reached, the memory appears to be about 100 ns FWHM, which is certainly not very appealing for high flux operation (although still smaller than for conventional MWPCs). Possible ways of reducing the memory will be discussed in the last section. Notice that the resolution time of the chamber, i.e. the time jitter of the detected tracks, is much smaller than the memory, and a good recording of the time of detection should allow the improvement of background rejection. The best resolution times in the GMSC have been measured operating in the conversion off condition with 30 ns gate, and discriminating the detected signal after a double differentiation (a simple method of peak-time measurement). A typical time spectrum obtained in these conditions is shown in fig. 13 and has 10 ns FWHM; the presence of tails is again a manifestation of the large non-Gaussian fluctuations due both to the primary pair statistics and to the avalanche size.

The efficiency plateaux shown in fig. 10 were obtained at a moderate beam flux (below 10^3 s^{-1} mm^{-2}). As already discussed in section 4, spontaneous breakdown on the beam spot is observed at high gains and particle rates, thus limiting the maximum operational voltage of the detector. The effect is particularly large in the d.c. open gate condition, as already discussed. In fig. 14 typical efficiency curves (measured at very low rate) and flux-dependent breakdown voltages are shown in the conversion off, open gate operation; for rates above 10^3 s^{-1} mm^{-2} full efficiency cannot be reached, owing to breakdown. Two sets of points are measured for different preamplification factors.

Much higher gains can be reached before breakdown at a given flux in the fully gated operation of the GMSC. This is shown in figs. 15 and 16 for the conversion on and off operation, respectively. As for the previous figure, efficiency plateaux are given as a function of V_2 for several values of V_1, and the breakdown voltage in the second amplifying element is shown as a function of particles' flux. The experimental bars for the breakdown voltage cover the possible range of the gating frequency, from 10^4 s^{-1} to zero; the last point corresponds obviously to the natural breakdown of the single gap without transfers. At large fluxes, this intrinsic limit is reached also in the first amplifying element, and the figures close to the experimental bars indicate the value of V_1 at which the measurement was performed; at each rate, the proper efficiency plateau has to be considered. For example, in fig. 16, at a flux of 2×10^5 s^{-1} mm^{-2}, V_1 can be increased up to 3.25 kV, and breakdown occurs at V_2 = 3.05 kV; the corresponding maximum efficiency is then around 90% as read on the V_1 = 3.25 kV curve. No noticeable difference in the efficiency plateau shape was observed at increasing particle fluxes, proving that space-charge gain reduction, such as that observed in normal MWPCs, is absent in the GMSC, as already mentioned. We had indeed mounted in the same beam a conventional MWPC, having 2.54 mm anode wire spacing, to be used as a positional accuracy monitor (see the next section): typical efficiency plateaux obtained in the MWPC at increasing beam fluxes as a function of anodic voltage are shown in fig. 17. The maximum efficiency is already reduced to 90% at a flux of 3.5×10^4 s^{-1} mm^{-2}, and this has limited our study of the GMSC localization properties to moderate beam rates.

6. LOCALIZATION PROPERTIES OF THE GMSC

The large avalanche spread in our particular low-quenched gas mixture is responsible for the observed preamplification and transfer properties of the multistep avalanche chamber; in the gas mixture used in the present work, 2% acetone in argon, the standard deviation of the electron avalanche for one step of multiplication is about 300 μm [6]. For a double step multiplication process as in the GMSC, also on account of diffusion in the drift regions, a transverse charge

extension at the last electrode having about 700 μm standard deviation is observed[13]. As a consequence, several wires in the last plane share the detected charge and, as noticed in a similar case for MWPC, the position accuracy obtained with a centre-of-gravity measurement is better than the wire spacing itself[11,12]. When recording the fast component of the negative signal on the electrode, however, a compensation mechanism similar to the one observed on the anodes of MWPCs takes place. Indeed, electrons collected by one wire, and producing there a negative signal, induce a positive charge on the adjacent wires that overlaps with and partially compensates the direct electron signal; as a result, the spatial extension of the fast induced signal is considerably smaller (about a factor of two) than the true electron avalanche width. A typical induced signal pulse-height distribution for a single event, measured on the last electrode of a GMSC with the method outlined in section 2, is shown in fig. 18; each horizontal bin corresponds to one wire spacing, 500 μm, and the distribution has a standard deviation of about 0.4 mm. The variance of the avalanche width, measured on a large sample of events, is very small, 1/25 of a bin size, or 20 μm; the analysis of the avalanche width should be a powerful tool in case of multiparticle or jet events. The reduction of the measured over the physical width is particularly interesting if one considers the two-track separation allowed by the detector; from the figure, one would expect to identify two tracks about 1.5 to 2 mm apart. As an example, fig. 19 shows the pulse-height distribution measured for an event having two simultaneous tracks 2.5 mm apart and recorded during the high-flux measurements previously described. Figure 20 shows instead an event that may correspond to two tracks 1 mm apart, and with the pulse-height spectra partially overlapping. The analysis of this kind of event with a single detector is however difficult and has not been attempted yet, in particular concerning the position distortion due to the partial overlap of the induced signals' distribution. Notice that in the pulse-height spectra of figs. 18 to 20 the ADC pedestal, a presettable d.c. level at the input of the converters, has been subtracted following the procedure outlined in ref. 12; this results in measured amplitudes below the base line for

all channels adjacent to the ones of the peak, because of the opposite polarity signals induced on the GMSC wires by the charge-compensating mechanism described above. In computing the centre of gravity of the distribution, only the cluster of adjacent significative channels above the base line have been taken into account.

The localization properties of the GMSC have been checked using a collimated ^{55}Fe X-ray beam and operating the device in the self-gated mode. The centre-of-gravity distribution as measured for two beam positions 3 mm apart is shown in fig. 21; the physical width of the collimated beam, about 500 μm in diameter, gives of course the major contribution to the measured dispersion. The observed width of the distribution, having a standard deviation of about 200 μm, can only be justified by an intrinsic localization accuracy in the 100 μm region, thus proving that, at least for a localized charge cluster such as the one provided by 5.9 keV X-rays, the large avalanche spread takes place in a rather symmetric way.

The position accuracy in the detection of charged particles is normally best analysed using a triplet of identical detectors. This could not be done however in our test run, and we have installed on line a normal MWPC with 2.54 mm anode wire spacing, used in the drift mode, as positional reference. The time of detection of the beam particles triggering the GMSC system was recorded in a set of time-to-digital converters, and assumed to be proportional to the distance of the track from the MWPC wires; owing to the small beam size, only two wires in the MWPC were actually read out. A linear dependence of the drift-time on the distance was assumed, with a slope of 20 ns mm^{-1}, as often verified in similar conditions for tracks perpendicular to the anode wire plane, with intrinsic localization accuracies equal to or better than 100 μm [15]. Obviously, the same time of drift is measured for tracks on both sides and at equal distances from an anode wire (the right-left ambiguity). Figure 22 shows the correlation plot between the beam tracks' coordinates measured through the centre-of-gravity calculation in the GMSC (horizontal axis) and the drift-time measured on the two wires of the MWPC (vertical axis). Data for the GMSC correspond to the conversion off, 30 ns gate

operating condition; as already emphasized, this correlated measurement could only be performed at low beam flux ($\sim 10^3$ s^{-1} mm^{-2}) because of the rate limitations in the MWPC. The gating frequency for the GMSC was in this case limited to about 200 s^{-1} by the data acquisition link.

The localization accuracy in the GMSC is clearly good enough to separate the right and left tracks in the MWPC, at least for events not too close to the anode wires. A projection of the two-dimensional scatter plot for events in a slice 2 ns wide around the centre of the drift-time distribution is shown in fig. 23; each peak has a standard deviation of around 200 μm, which includes of course both the contributions of the MWPC and of the GMSC. From the previous considerations, it is inferred that the localization accuracy of the GMSC for minimum ionizing particles is about 150 μm.

When plotting the centre-of-gravity distribution for unselected events in the GMSC, fig. 24, a modulation effect appears with an amplitude corresponding to about ±50 μm (too small to be disclosed by the previous correlation). The modulation is probably due to the discrete structure of the multiplying grids or of the read-out electrodes; a similar behaviour was already noticed in ref. 4. Further study of the modulation effect is however required before attempting a non-linear correction of the data with the aim of improving the localization accuracy of the device.

7. SUMMARY OF THE RESULTS AND FUTURE DEVELOPMENTS

We have shown that, at least for moderate chambers' size, the problems connected with capacitive pick-up of the gating pulse from the sensitive electrodes can be solved by a proper grounding and by the use of a symmetric bipolar pair of gates. The residual pick-up is not much higher than the amplifiers' noise, and furthermore is several hundred nanoseconds in advance of the physical signal. Full efficiency of detection can be obtained for minimum ionizing particles in various operating conditions, the more stringent one corresponding to the conversion off, 30 ns gate width; the resolution time in this case is of about 10 ns FWHM, with a memory around 100 ns. No gain reduction due to space charge is

observed at increasing radiation fluxes; however, spontaneous breakdown in the beam region appears at a well-defined gain for a given flux, thus limiting the maximum operational voltage. Strong evidence suggests that breakdown is due to a mechanism of secondary extraction at the cathodes due to the positive ions' charge density. With the electronics sensitivity used, about 0.05 pC at the wires, full efficiency of detection for minimum ionizing particles can be reached up to maximum fluxes slightly in excess of 10^5 s^{-1} mm^{-2}, which is an order of magnitude more than in a conventional MWPC.

May we emphasize here that breakdown in a multistep avalanche chamber has no dramatic consequences, except for a short dead-time due to the power supplies' recovery time (that can be reduced to a few milliseconds); all electrodes in the structure are indeed realized with thick wire grids or meshes, contrary to the MWPC case, and the electronics can be protected by a pair of fast clamping diodes at the input, at least for moderate chambers' capacities.

The localization properties of the GMSC are rather unique, because of the large avalanche spread in the gas (about 1 mm FWHM). Charge interpolation is automatically performed, and a position accuracy of 150 μm standard deviation has been measured by recording the induced charge distribution on the last anode wires, 500 μm apart. Obviously, simpler digital on-wire electronics can be used, similar to the systems developed for MWPCs, and one would then expect an accuracy comparable with the wire spacing. This last parameter can be varied in a large range, since in the parallel-plate avalanche mode of amplification the wires' diameter and distance play no role (as long as their surface field is not too large).

Although this has not been implemented in the chamber described, two-dimensional or multi-dimensional localization can be obtained in the multistep devices by transferring part of the electron charges in the last avalanche to another electrode, at an angle with the previous one; the transfer properties of such structures are indeed well understood. In particular, the last electrode in the chamber can be made with a printed circuit, where any convenient read-out pattern can be implemented.

In the formation of the induced signal on a set of adjacent wires, a compensation phenomenon appears, reducing the measured fast-charge distribution to about half of the physical electron avalanche size: this is particularly convenient to improve the two-track separation that has been shown to be of around 2 mm. Also, the presence of signals of opposite polarity on the tails of the induced signal distribution sharpens the transition from a significative signal to the background level, thus eliminating the common problem of low-level tails in the centre-of-gravity calculation.

The major drawback of the GMSC lies in its long memory time, around 100 ns, due to the extended longitudinal avalanche size. It is obviously easy to reduce this size, by increasing the amount of quencher, as shown for example by fig. 2 of ref. 6; however, the uniform transfer properties of the preamplification element are quickly degraded when the avalanche size is reduced below the transfer grid wire spacing. With the meshes we have used, having 0.5 mm pitch, the minimum avalanche size for correct behaviour has around 200 μm standard deviation. We are currently investigating the possibility of using finer grids or micromeshes, which would allow a good transfer for smaller avalanche size.

It seems also desirable to improve the GMSC time resolution over the measured one, 10 ns FWHM. The reduction in the avalanche size is expected to reduce its fluctuations, but the intrinsic limit of the present design is given by the statistics of the primary ion-pair production in the gap. Use of heavier gases (xenon replacing argon) or of pressures higher than atmospheric should, by the increase of the ionization density, remove part of the statistical fluctuation, and we are investigating in this direction.

Several parameters need however to be improved to make the GMSC a useful device, for example in selective high flux beam localization. We are, in particular, investigating in detail the breakdown mechanism, and its dependence on the gas and the electrodes' nature; lowering the discrimination threshold (which was not particularly low for the described measurement) could be another way of improving the rate capability of the GMSC, by allowing operation at a lower voltage.

REFERENCES

1) G. Charpak, G. Melchart, G. Petersen, F. Sauli, E. Bourdinaud, P. Blumenfeld, C. Duchazeaubeneix, A. Garin, S. Majewski and R. Walczak, New approaches in high-rate particle detection, CERN 78-05 (1978).

2) R.W. Hendricks, Rev. Sci. Instrum. 40 (1969) 1216.

3) G. Charpak and F. Sauli, Phys. Lett. 78B (1978) 523.

4) A. Breskin, G. Charpak, S. Majewski, G. Melchart, G. Petersen and F. Sauli, Nucl. Instrum. Methods 161 (1979) 19.

5) G. Charpak, G. Melchart, G. Petersen and F. Sauli, IEEE Trans. Nucl. Sci. NS-26 (1979) 186.

6) G. Melchart, G. Charpak and F. Sauli, IEEE Trans. Nucl. Sci. NS-27 (1980), 124.

7) G. Charpak, S. Majewski, G. Melchart, F. Sauli and T. Ypsilantis, Nucl. Instrum. Methods 164 (1979) 419.

8) J. Séguinot, J. Tocqueville and T. Ypsilantis, Imaging Čerenkov detector: photoionization of triethylamine, preprint CERN-EP/79-161 (1979), submitted to Nucl. Instrum. Methods.

9) G. Petersen, G. Charpak, G. Melchart and F. Sauli, The multistep avalanche chamber as a detector in radiochromatography imaging, CERN-EP/80-39 (1980), presented at the Wire Chamber Conference, Vienna, February 1980.

10) R. Bouclier, G. Charpak, G. Million, J.C. Santiard and F. Sauli, Technological developments for the construction of the multistep chambers and of the associated electronics, to be published.

11) G. Charpak, G. Petersen, A. Policarpo and F. Sauli, Nucl. Instrum. Methods 148 (1978) 471.

12) G. Charpak, G. Melchart, G. Petersen and F. Sauli, Nucl. Instrum. Methods 167 (1979) 455.

13) G. Charpak, F. Mathy, A. Peisert and F. Sauli, Detailed study of the properties of avalanche growth and distribution in the multistep avalanche chamber, to be published.

14) F. Sauli, Principles of operation of multiwire proportional and drift chambers, CERN 77-09 (1977), and references therein.

15) G. Charpak, F. Sauli and W. Duinker, Nucl. Instrum. Methods 108 (1973) 413.

Figure captions

Fig. 1 : Schematics of the gated multistep avalanche chamber (GMSC). Electrodes identified by the potentials HV2, HV3, and GND are crossed wire meshes, having 50 μm wire diameter and 500 μm pitch. Electrodes HV4-HV5 and HV6 are planes of parallel wires, with diameter and pitch as before, perpendicular to each other; the particular layout of the gate electrode allows to d.c. or pulse offset pairs of adjacent wires. Electrode HV1 is a 10 μm thick aluminium foil. By a proper choice of potentials, charges liberated in the conversion region are preamplified and transferred to drift region 1; if the gate electrode is equipotential at the time the electron cloud approaches, the charge is transferred to the second element of amplification, equipped with read-out electronics.

Fig. 2 : The absolute gain in a 5 mm thick parallel-plate chamber, operated at atmospheric pressure in a 98-2 mixture of argon-acetone, as a function of the applied field.

Fig. 3 : Transparency for electrons of the gate electrode, as a function of the difference of potential V_G = (HV4 - HV5) between adjacent pairs of wires (500 μm pitch). The voltage difference for blocking, about 180 V, depends of course on the existing drift field, 1.4 kV/cm as can be deduced from the values indicated in the inset.

Fig. 4 : Over-all system transparency, detected at the last electrode, for an equipotential gate as a function of its voltage; a large region of uniformity exists.

Fig. 5 : Two identical avalanche transistor circuits are used to generate the pair of symmetric gating pulses (one only is shown in the figure; in the second the transformer winding and the output diodes are inverted). The pulse duration can be adjusted varying the length of the shaping cable L. The gate electrode is represented by the capacitive load C; the diodes in the output protect the transistors from accidental overvoltage in case of spark breakdown in the chamber.

Fig. 6 : Shape observed on the chamber of the gating pulses, for 60 ns and 30 ns shaping constants, respectively. The vertical axis is attenuated on the scope by a factor of 20.

Fig. 7 : Gate transmission in the pulsed mode of operation as a function of the gate delay, relative to the migrating electron cloud and for several shaping constants. The measurement has been done irradiating the GMSC with a ^{55}Fe X-ray source and detecting the preamplified pulse to generate the gate pulse. The transmission efficiency is defined as the ratio of the detected pulse height in the last electrode for a gated and for a d.c. open operation.

Fig. 8 : Pick-up of the gating pulse on the read-out electrode. In (a) the upper trace (with 5 mV/division sensitivity) shows the signal detected on the preamplification element for a 5.9 keV X-ray, used to trigger the gate pulse, and the lower trace (500 mV/division) the charge detected on the last electrode after gating and amplification. Since the upper meshes in fig. 1 are not screened from the gate electrode, a large pick-up swing appears at the time of pulsing on the preamplification element. The pick-up on the main amplification grid is however much smaller, as shown in (b) on a more sensitive scale (5 mV/division), and is easily discriminated.

Fig. 9 : The spark breakdown voltage in the second amplification element, for a fixed preamplification, as a function of the detected 8 keV X-ray flux. Measurements are shown both for the d.c. open gate condition, and for the pulsed gate operation; in the last case, the small figures on the two sides of the measurement bars indicate the gate opening frequency (as a percentage of the total flux detected on the preamplification element). The gated operation allows the attainment of chamber gains larger by almost two orders of magnitude (see fig. 2), also for opening frequencies approaching 100%, thus indicating that breakdown is caused by positive ions' feedback.

Fig. 10 : Efficiency plateaux for the detection of minimum ionizing particles, as a function of the voltage in the second amplification element, for several operating conditions. The conversion on mode corresponds to detection of the ionization produced in the conversion space, while in the conversion off only the charge produced within the preamplification element is multiplied. The two modes can be simply selected by a proper adjustment of HV1 (see fig. 1).

Fig. 11 : Pulse-height spectra for minimum ionizing particles, in the fully gated operation of the GMSC, in the conversion on (a) and off (b) conditions. The chamber gain in the second case has been increased by about a factor of 10.

Fig. 12 : Efficiency versus gate delay in the detection of minimum ionizing particles, in the conversion off condition and for several amplification voltages.

Fig. 13 : Time resolution of the GMSC for fast particles, measured with a double differentiation circuit on the signal detected on the last electrode. The horizontal scale is 10 ns/division.

Fig. 14 : Efficiency for detection of minimum ionizing particles, measured at small rates and for two values of preamplification (full lines and left vertical scale), and breakdown voltage as a function of particles' rate (broken lines and right vertical scales). Operating conditions for the GMSC: conversion off and gate d.c. open.

Fig. 15 : Same as for fig. 14, for the conversion on and 30 ns gate operation. The sparking point bars represent the measurement of breakdown, for a given flux, at two extremes of gate-opening frequencies (10 kHz and zero). The value of the preamplification voltage for each measurement is also shown, and the reading has to be combined with the corresponding efficiency plateau for a given flux.

Fig. 16 : Same as fig. 15, for a gated, conversion off operation.

Fig. 17 : Efficiency plateau for different beam fluxes measured in the MWPC used as a monitor for the measurement of accuracy. The efficiency reduction due to space charge is visible and has limited the use of the chamber to rates below $\sim 10^4$ s^{-1} mm^{-2}.

Fig. 18 : Pulse-height distribution for a single event measured in the GMSC on the last electrode after subtraction of the ADC pedestal. The channel width corresponds to the wire spacing, i.e. 500 μm.

Fig. 19 : Same as for fig. 18, for a double-track event; the distance between the two centres of gravity corresponds to about 2.5 mm.

Fig. 20 : Pulse-height distribution for an event probably corresponding to two tracks 1.5 mm apart.

Fig. 21 : Centre-of-gravity distribution measured in the GMSC for two positions of a collimated 5.9 keV X-ray source, 3 mm apart. The two peaks have a standard deviation of about 200 μm, which includes also the source collimation (200 μm full width).

Fig. 22 : Correlation plot between the centre of gravity of the signals induced on the last electrode of the GMSC, horizontal axis, and the time of drift measured on two adjacent wires of an MWPC for minimum ionizing particles.

Fig. 23 : Projection histogram of a horizontal slice 2 ns wide in the plot of fig. 22, for a time of drift in about the middle of the range. The standard deviation of the peaks, corresponding to the different right-left possibilities of the MWPC wires, is about 200 μm, including the localization accuracies of both the GMSC and of the MWPC used in the drift mode.

Fig. 24 : Histogram of the distribution of the centres of gravity measured for a large unselected sample of tracks in the GMSC; a modulation effect with a 500 μm period and about ±50 μm amplitude appears over the Gaussian-like beam distribution.

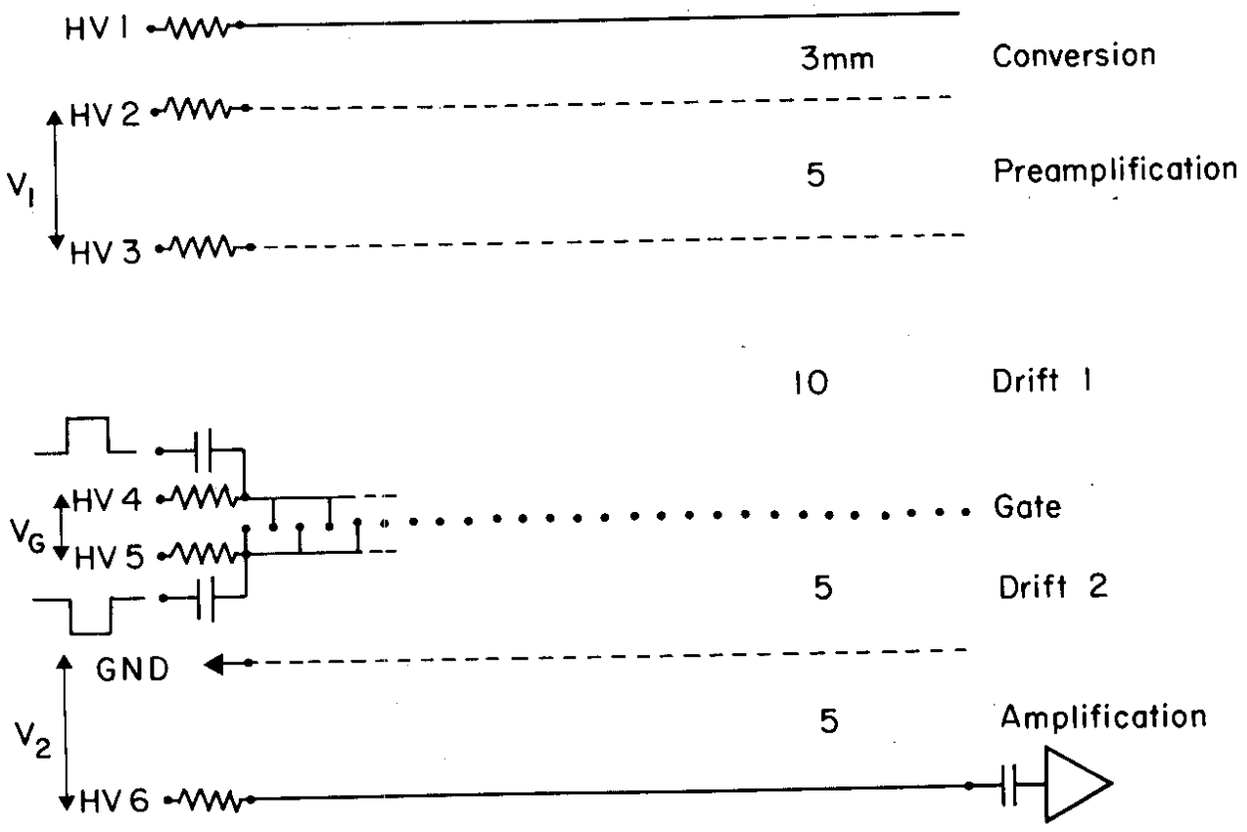
HV 1
3mm
Conversion
HV 2
V_1
5
Preamplification
HV 3
10
Drift 1
HV 4
V_G
Gate
HV 5
5
Drift 2
GND
5
Amplification
V_2
HV 6

Fig. 1

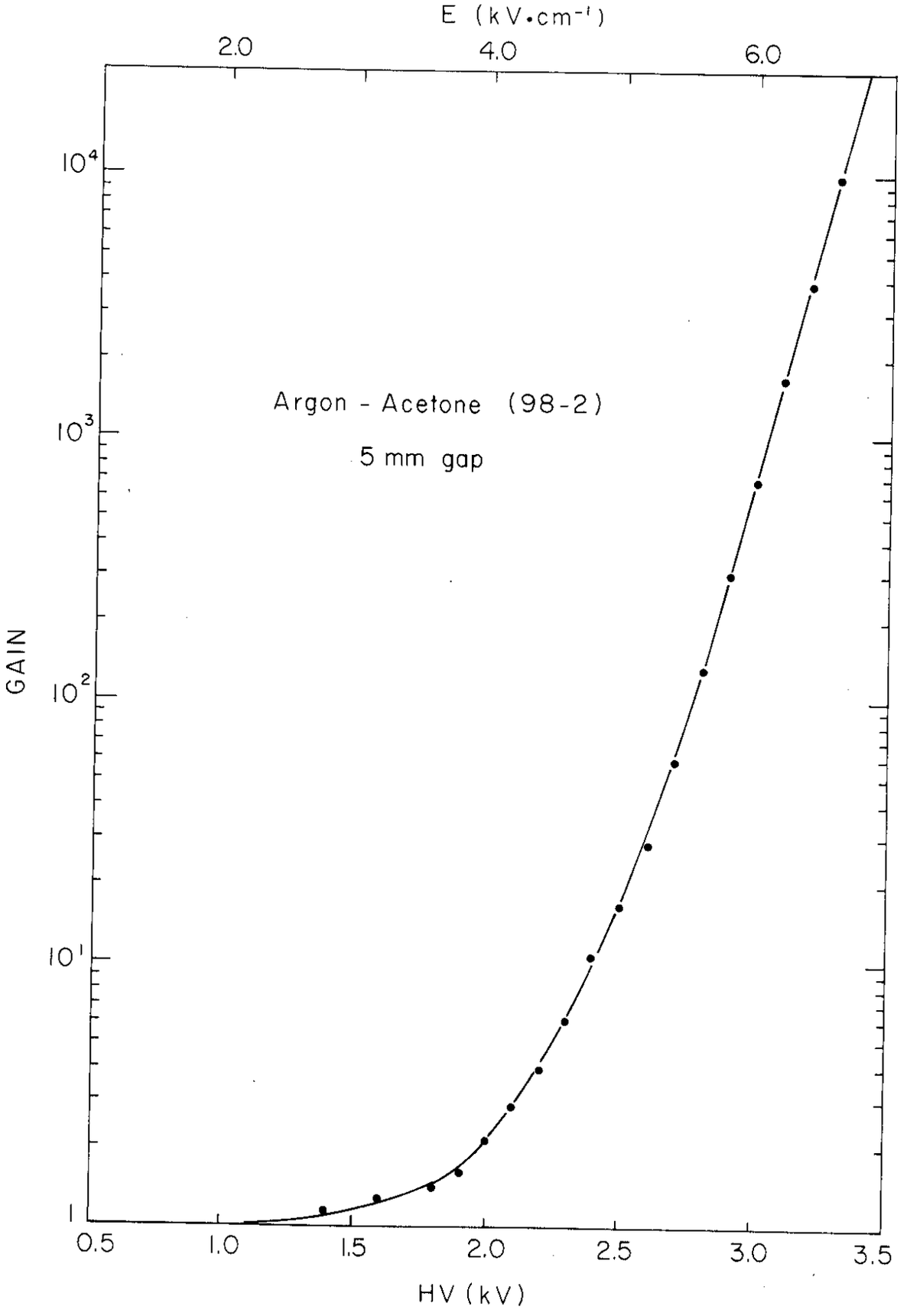
E (kV·cm⁻¹)
2.0
4.0
6.0
10⁴
10³
10²
10¹
1
GAIN
Argon - Acetone (98-2)
5 mm gap
0.5
1.0
1.5
2.0
2.5
3.0
3.5
HV (kV)

Fig. 2

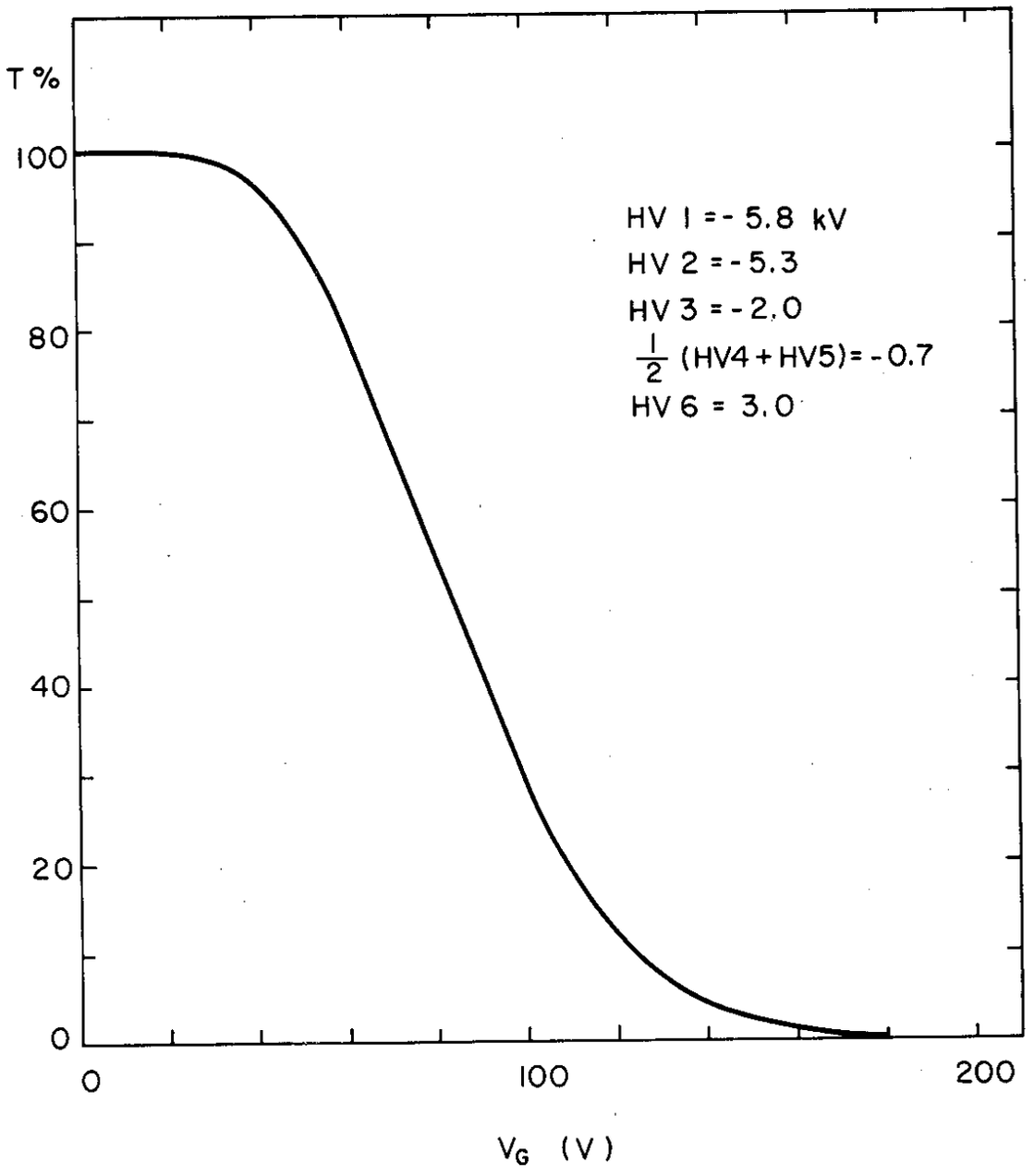
T %
100
80
60
40
20
0
0
100
200
V_G (V)
HV 1 = - 5.8 kV
HV 2 = - 5.3
HV 3 = - 2.0
$\frac{1}{2}$ (HV4 + HV5) = - 0.7
HV 6 = 3.0

Fig. 3

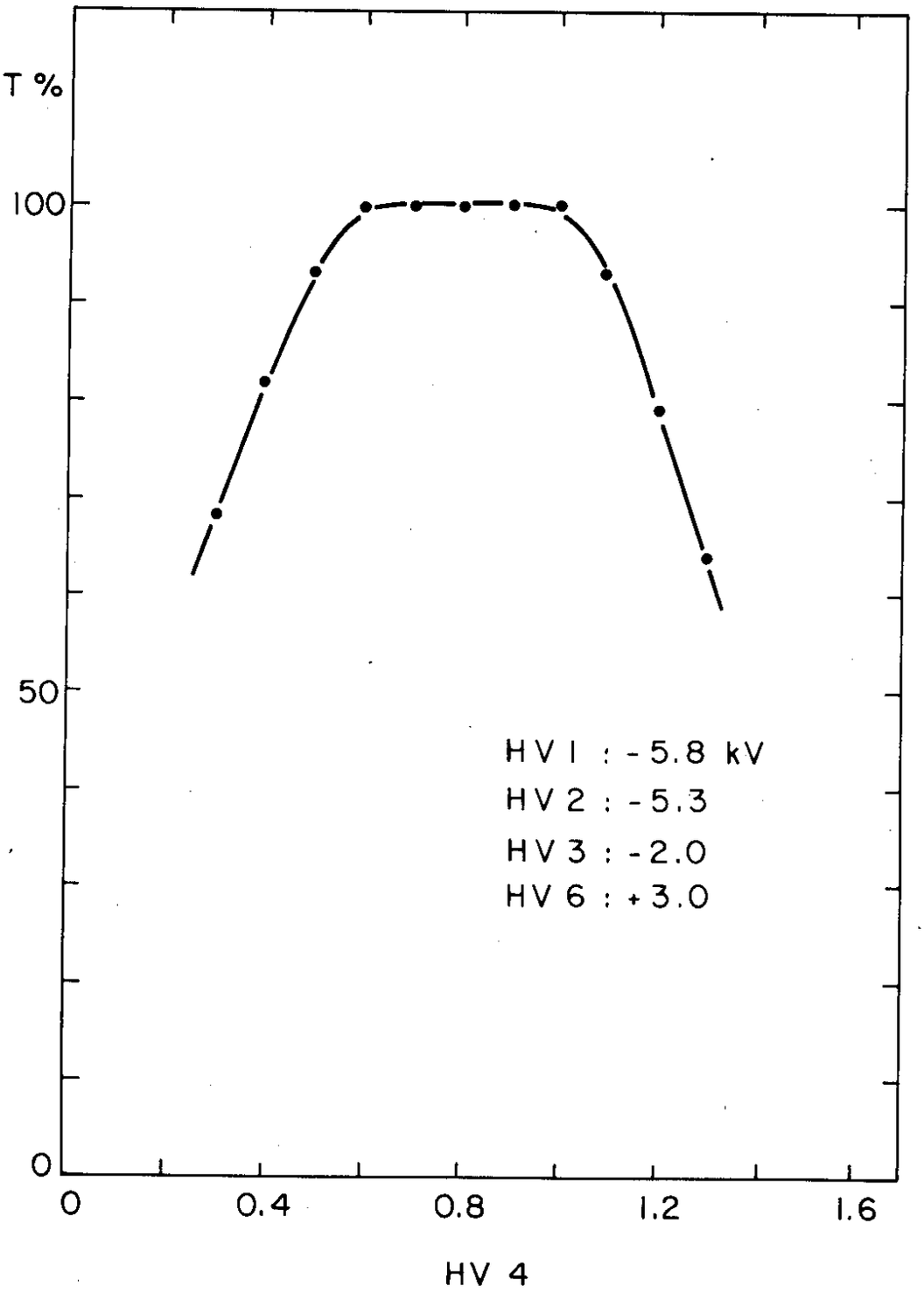

Fig. 4

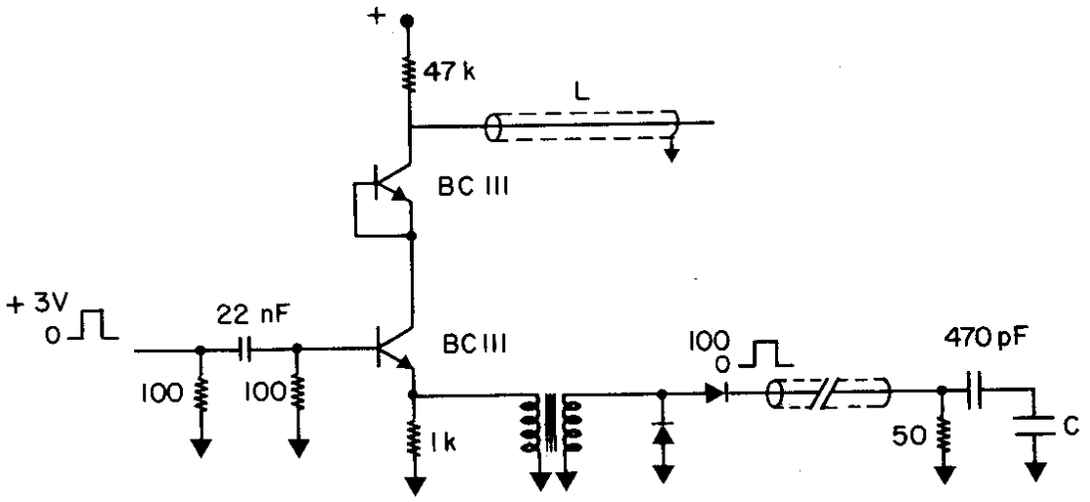

Fig. 5

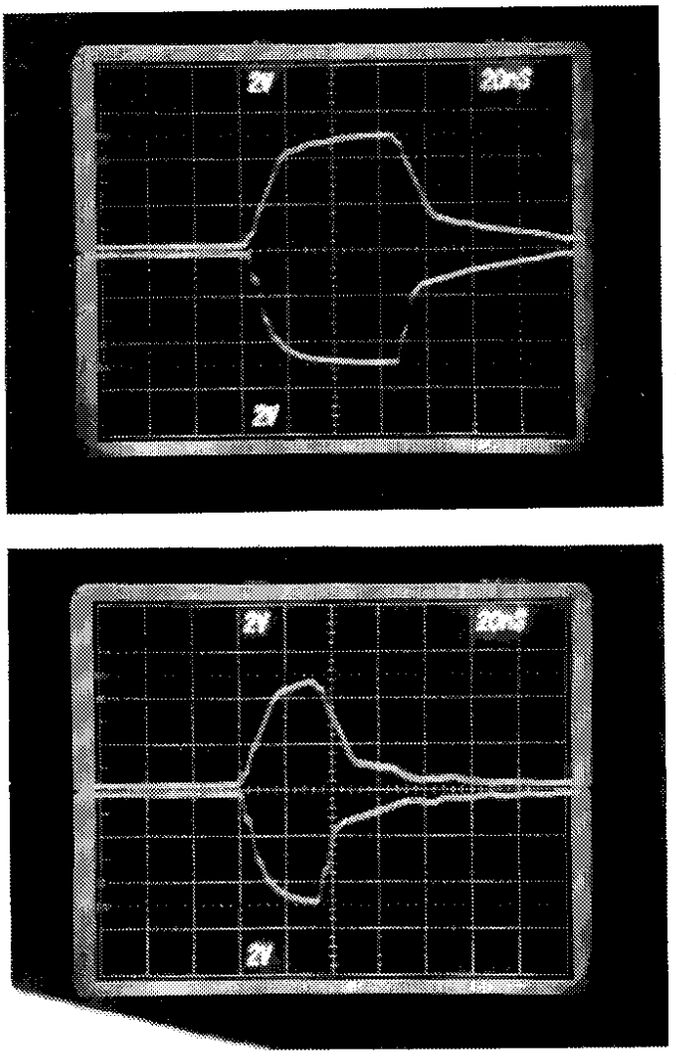

Fig. 6

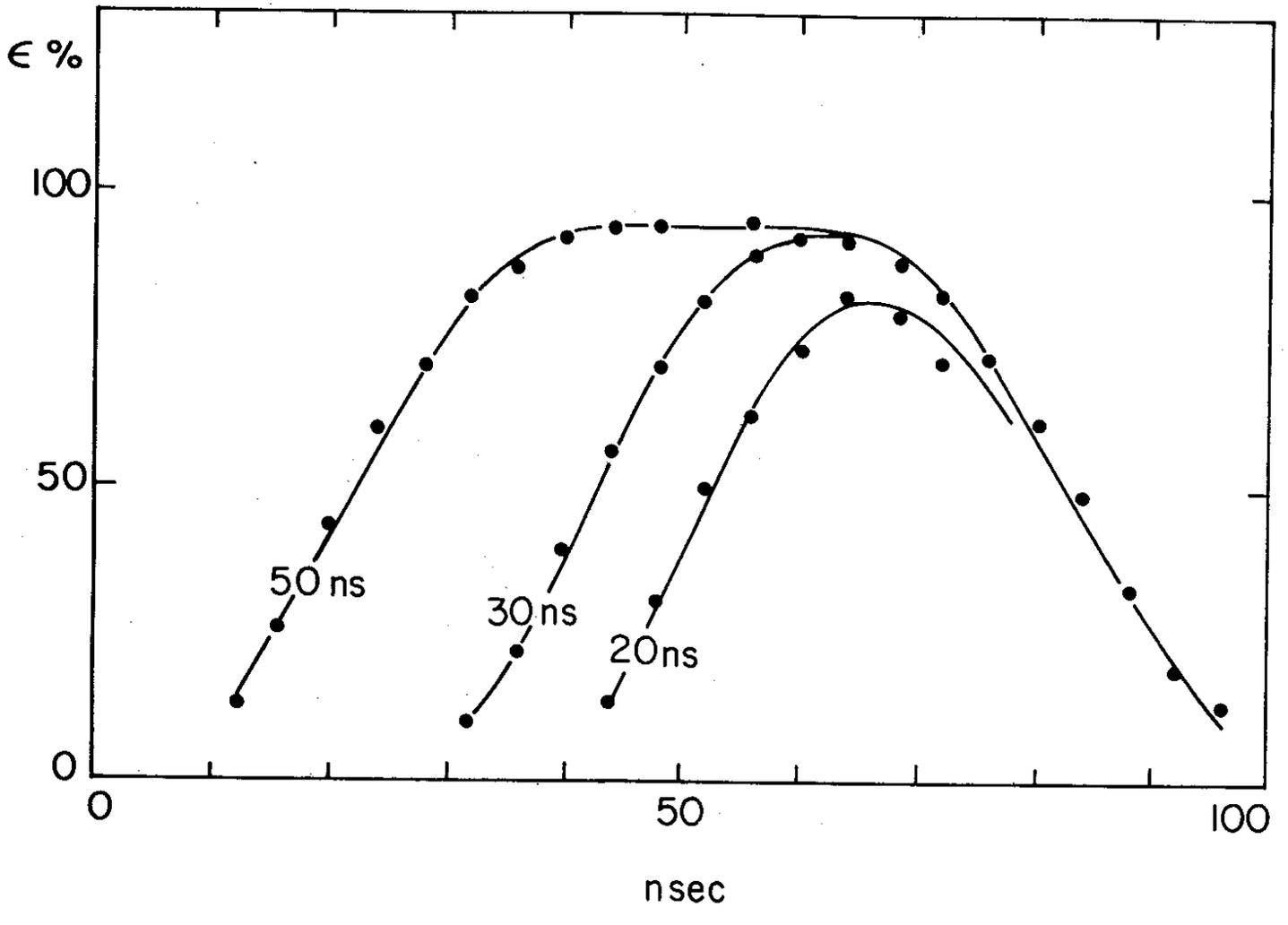

Fig. 7

a)

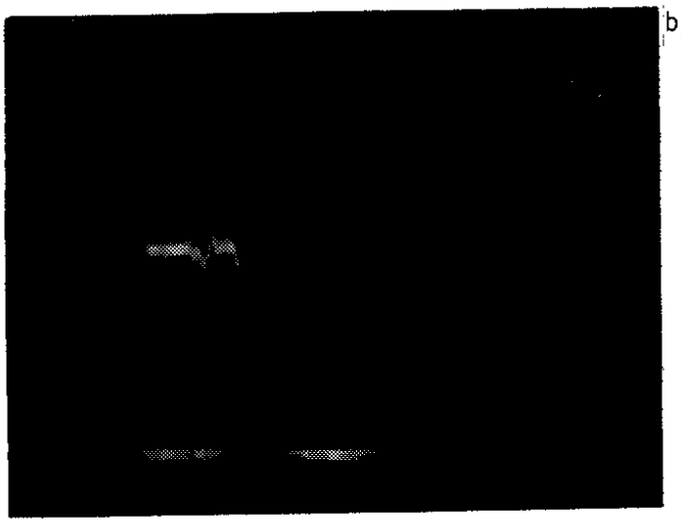

b)

Fig. 8

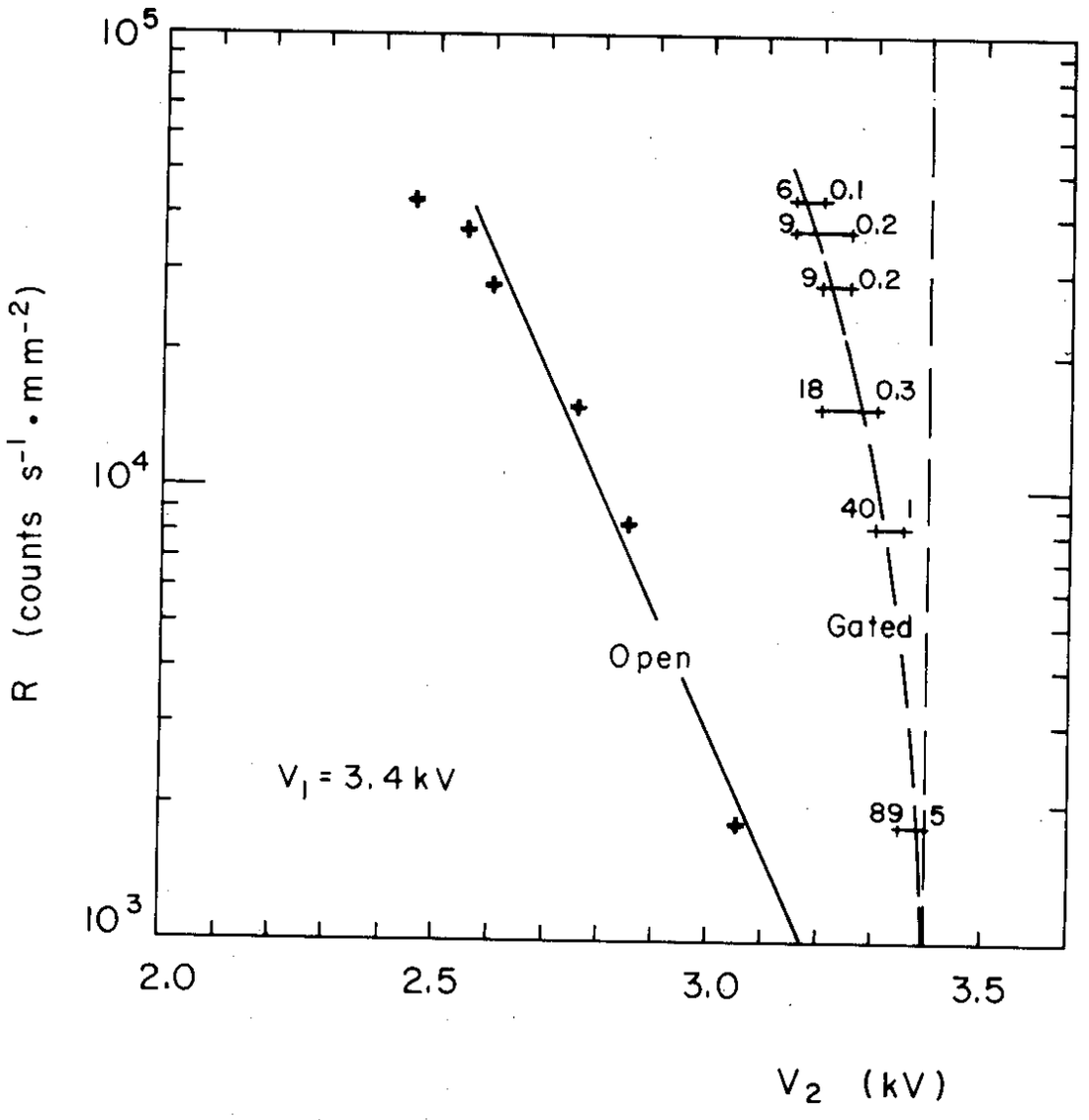
10^5
10^4
10^3
R (counts $s^{-1} \cdot m m^{-2}$)
2.0
2.5
3.0
3.5
V_2 (kV)
V_1 = 3.4 kV
Open
Gated
6
0.1
9
0.2
9
0.2
18
0.3
40
1
89
5

Fig. 9

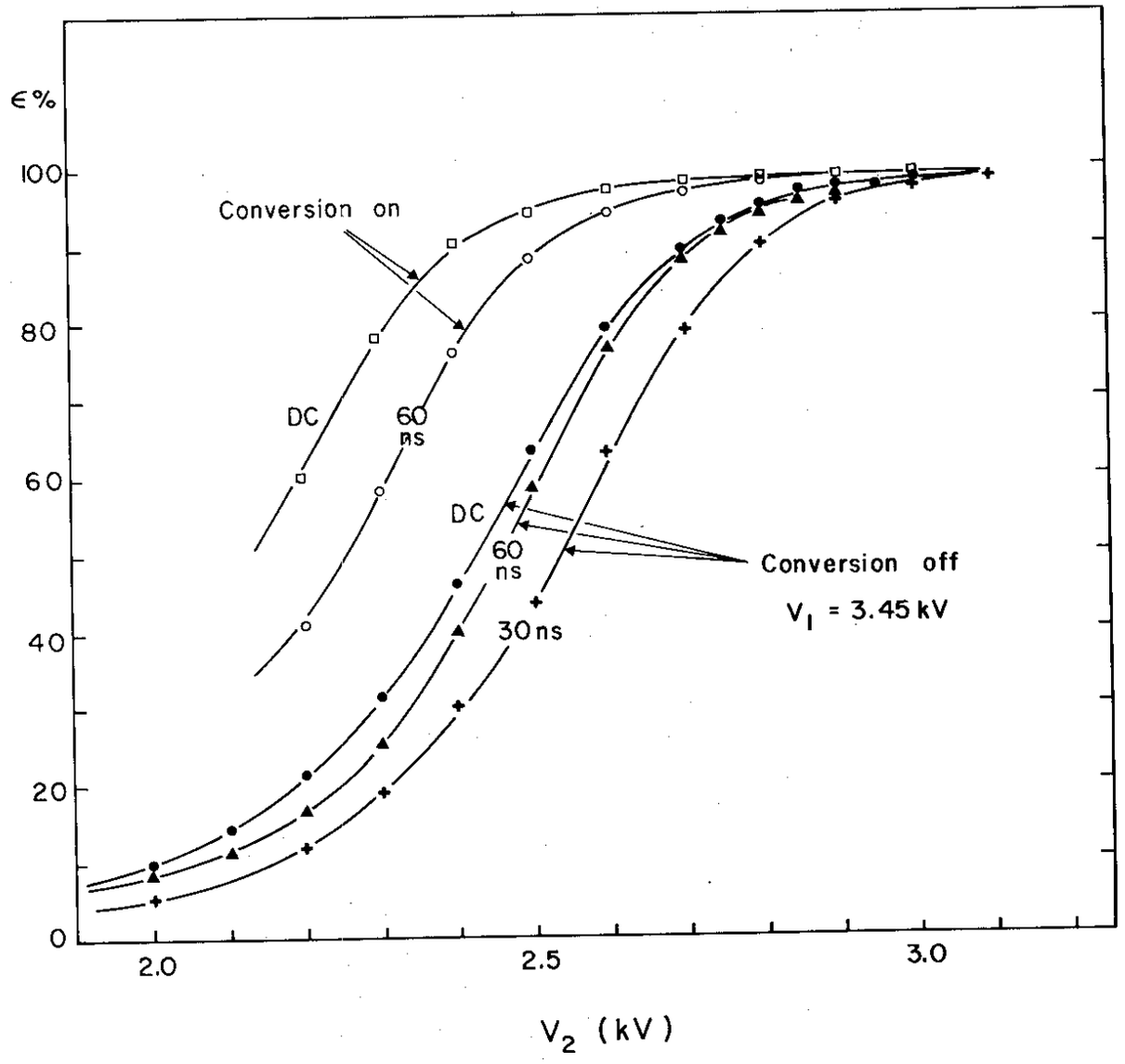
ϵ%
100
80
60
40
20
0
2.0
2.5
3.0
V_2 (kV)
Conversion on
DC
60 ns
DC
60 ns
30 ns
Conversion off
V_1 = 3.45 kV

Fig. 10

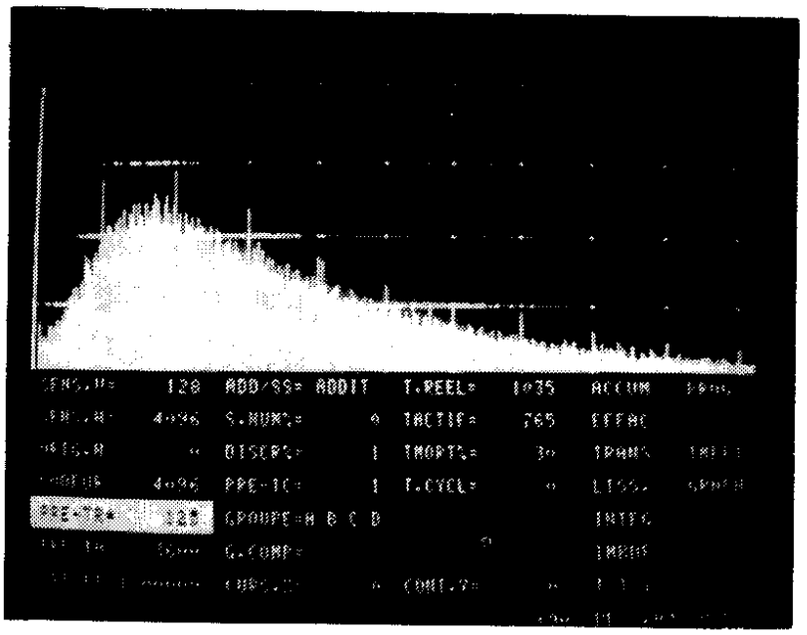
a)
ADD/SS= ADDIT
T.REEL= 1035
ACCUM
S.NUM%= 0
TRCTIF= 765
EFFAC
DISCR%= 1
TMORT%= 30
TRANS
PRE-TC= 1
T.CYCL= 0
LISS.
GROUPE=A B C D
INTEG
G.COMP=
INDOF
CURS.X= 0
CONT.Y= 0

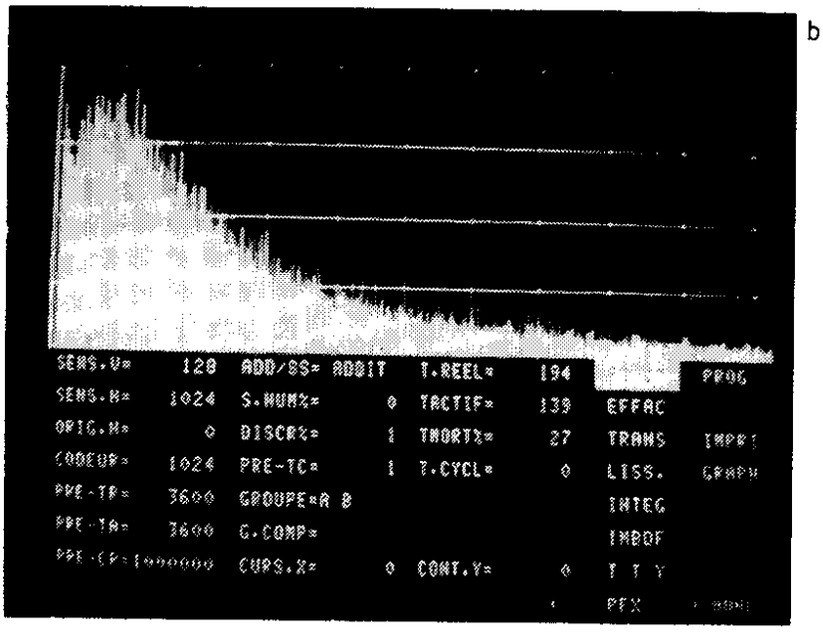
b)
SENS.V= 128
ADD/SS= ADDIT
T.REEL= 194
SENS.H= 1024
S.NUM%= 0
TRCTIF= 139
EFFAC
ORIG.H= 0
DISCR%= 1
TMORT%= 27
TRANS
CODEUR= 1024
PRE-TC= 1
T.CYCL= 0
LISS.
PRE-TP= 3600
GROUPE=A B
INTEG
PRE-TA= 3600
G.COMP=
INDOF
CURS.X= 0
CONT.Y= 0

Fig. 11

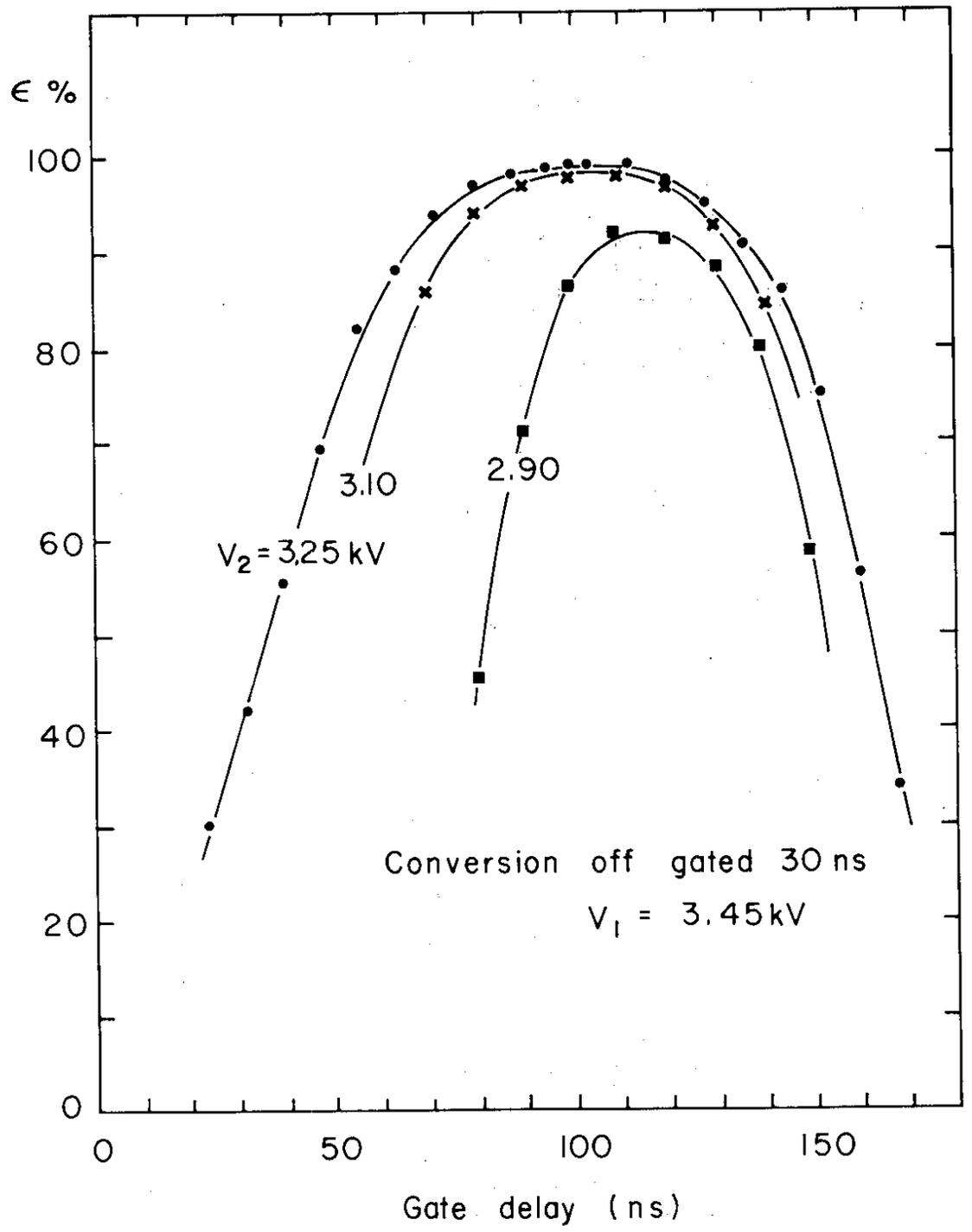
ϵ %
100
80
60
40
20
0
0
50
100
150
Gate delay (ns)
3.10
2.90
V_2 = 3.25 kV
Conversion off gated 30 ns
V_1 = 3.45 kV

Fig. 12

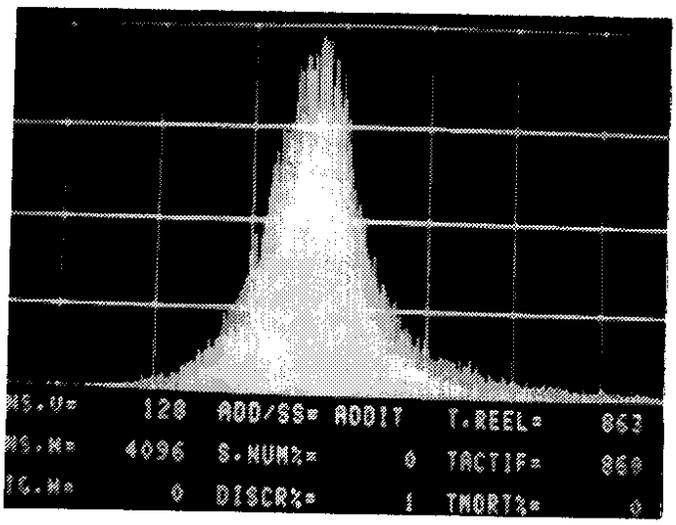
128 ADD/SS= ADD1? T.REEL= 852
4096 S.NUM%= 0 TACTIF= 860
0 DISCR%= 1 TMORT%= 0

Fig. 13

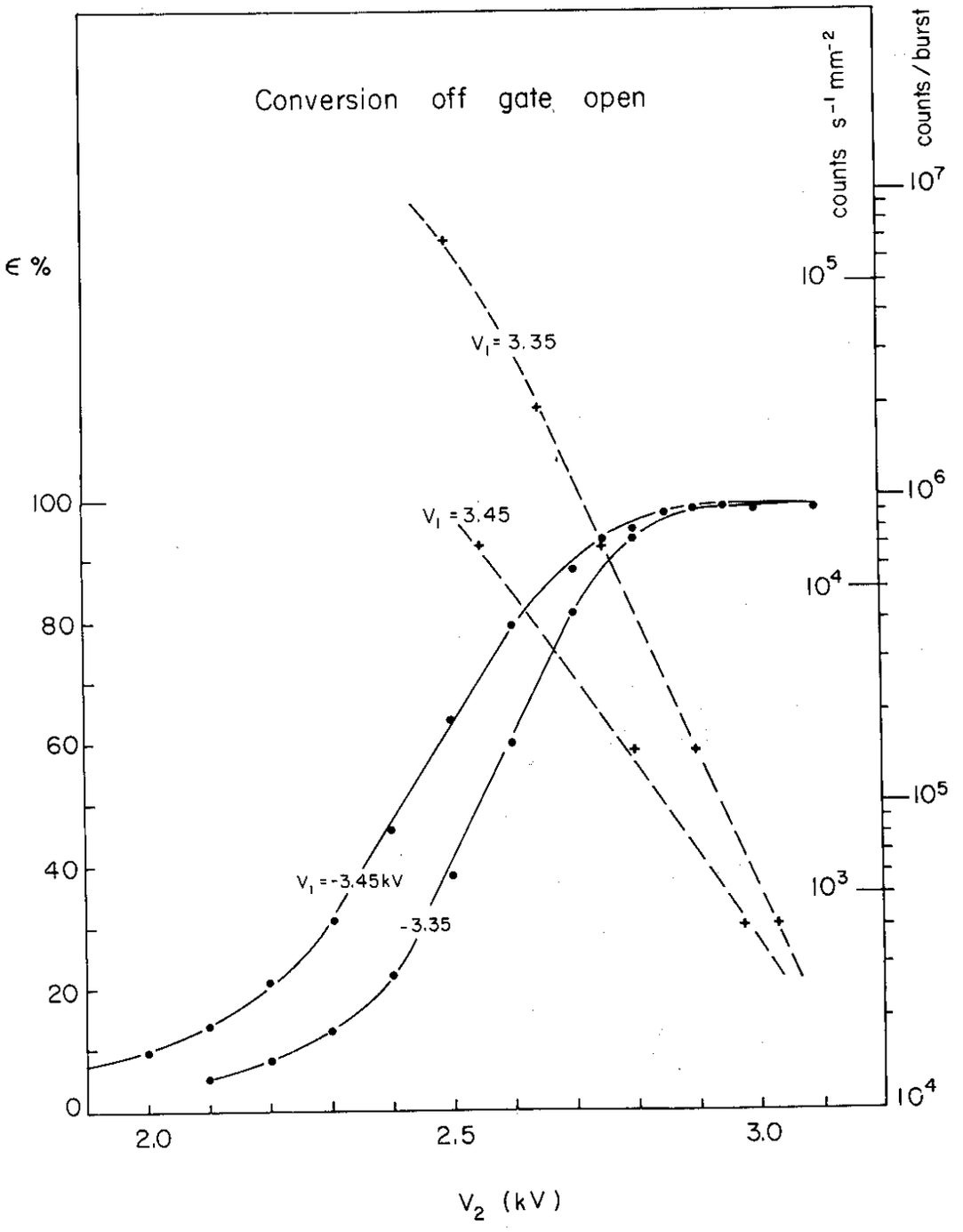
Conversion off gate open
ϵ %
counts s⁻¹ mm⁻²
counts / burst
V1 = 3.35
V1 = 3.45
V1 = -3.45kV
-3.35
100
80
60
40
20
0
10⁷
10⁶
10⁵
10⁴
10⁵
10³
10⁴
2.0
2.5
3.0
V2 (kV)

Fig. 14

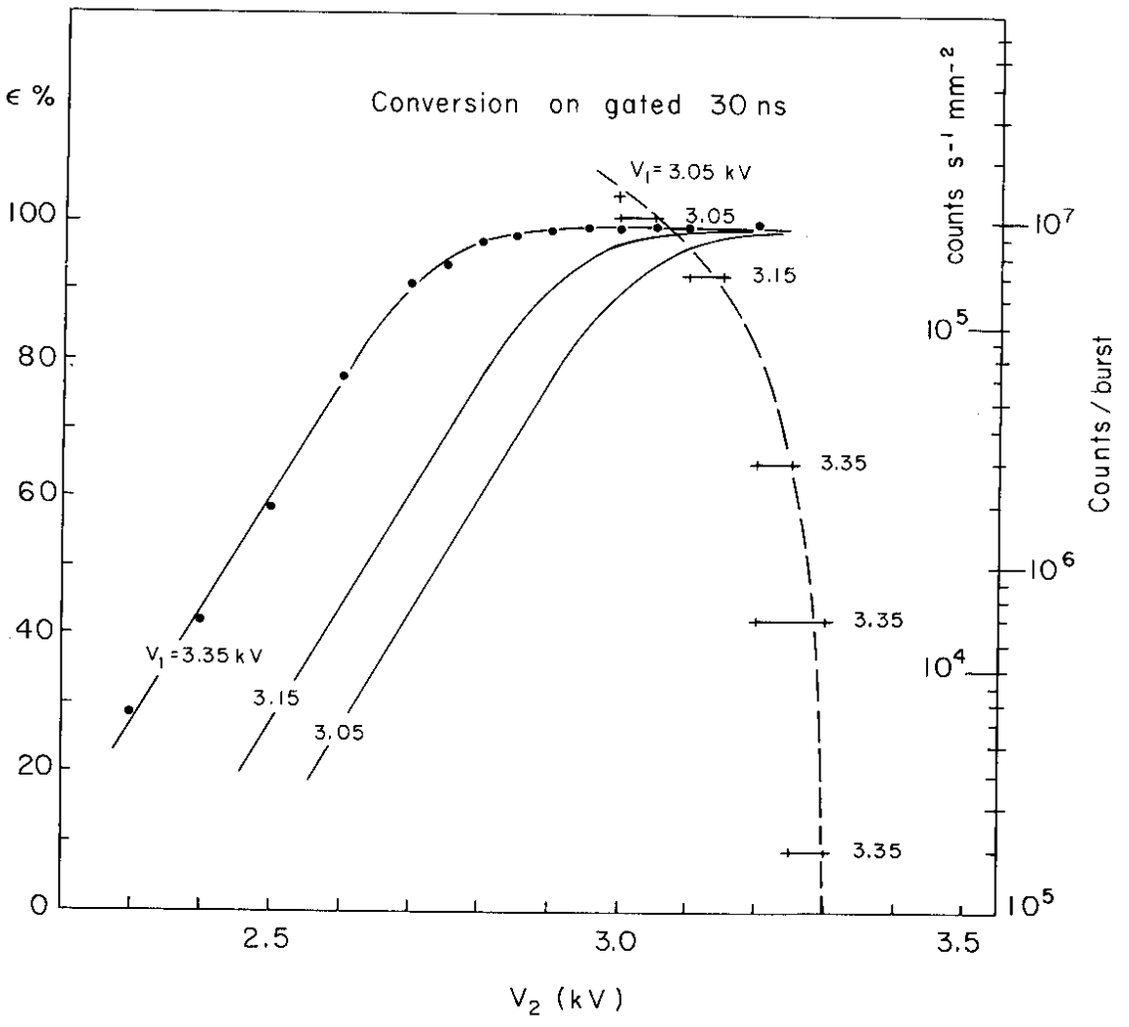
ϵ %
Conversion on gated 30 ns
V_1 = 3.05 kV
3.05
3.15
3.35
3.35
3.35
V_1 = 3.35 kV
3.15
3.05
100
80
60
40
20
0
2.5
3.0
3.5
V_2 (kV)
counts s^{-1} mm^{-2}
10^7
10^5
10^6
10^4
10^5
Counts / burst

Fig. 15

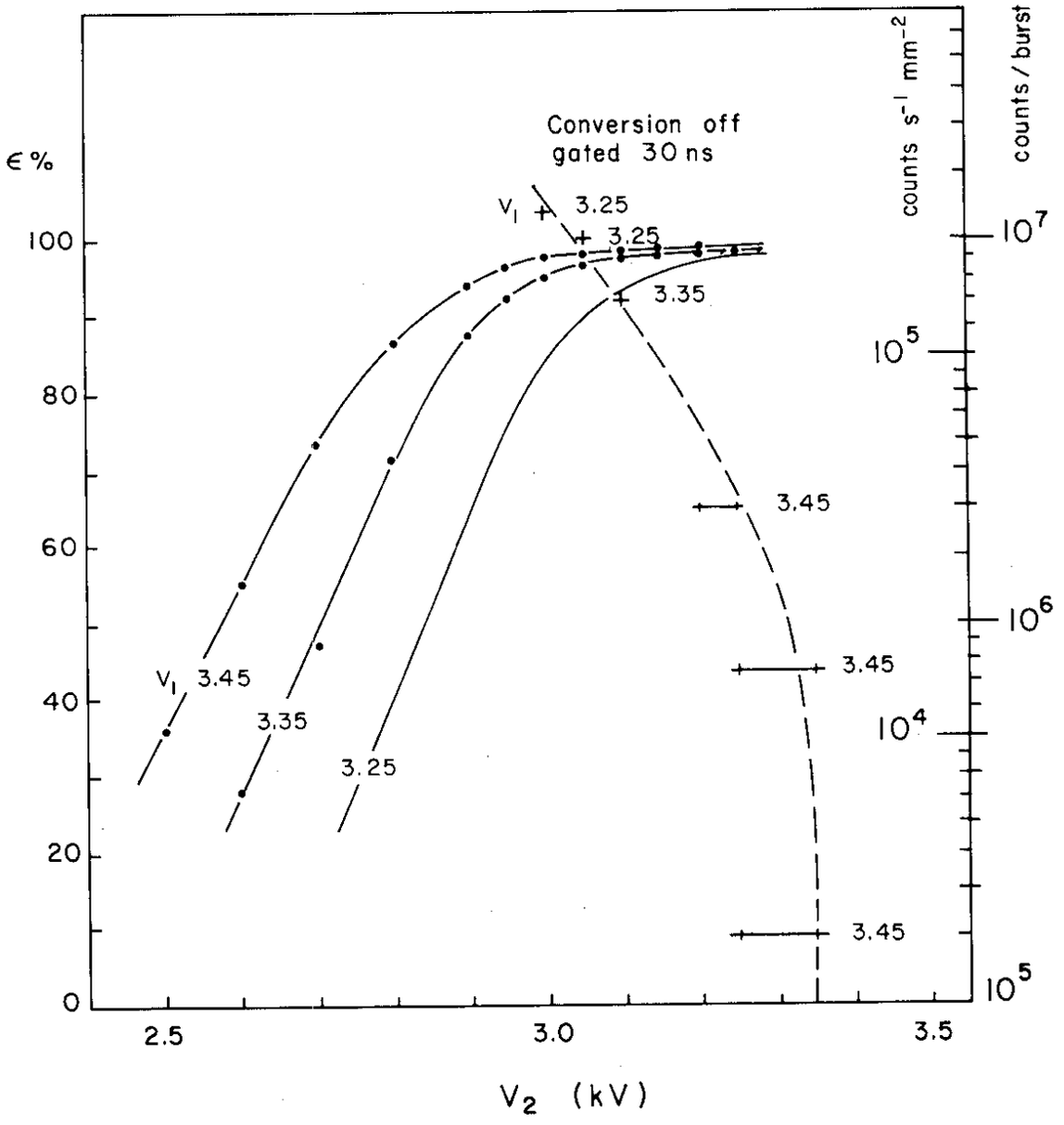
Conversion off
gated 30 ns
ε %
counts s⁻¹ mm⁻²
counts / burst
V1
3.25
3.25
3.35
3.45
3.45
3.45
3.45
3.35
3.25
100
80
60
40
20
0
10⁷
10⁵
10⁶
10⁴
10⁵
2.5
3.0
3.5
V2 (kV)

Fig. 16

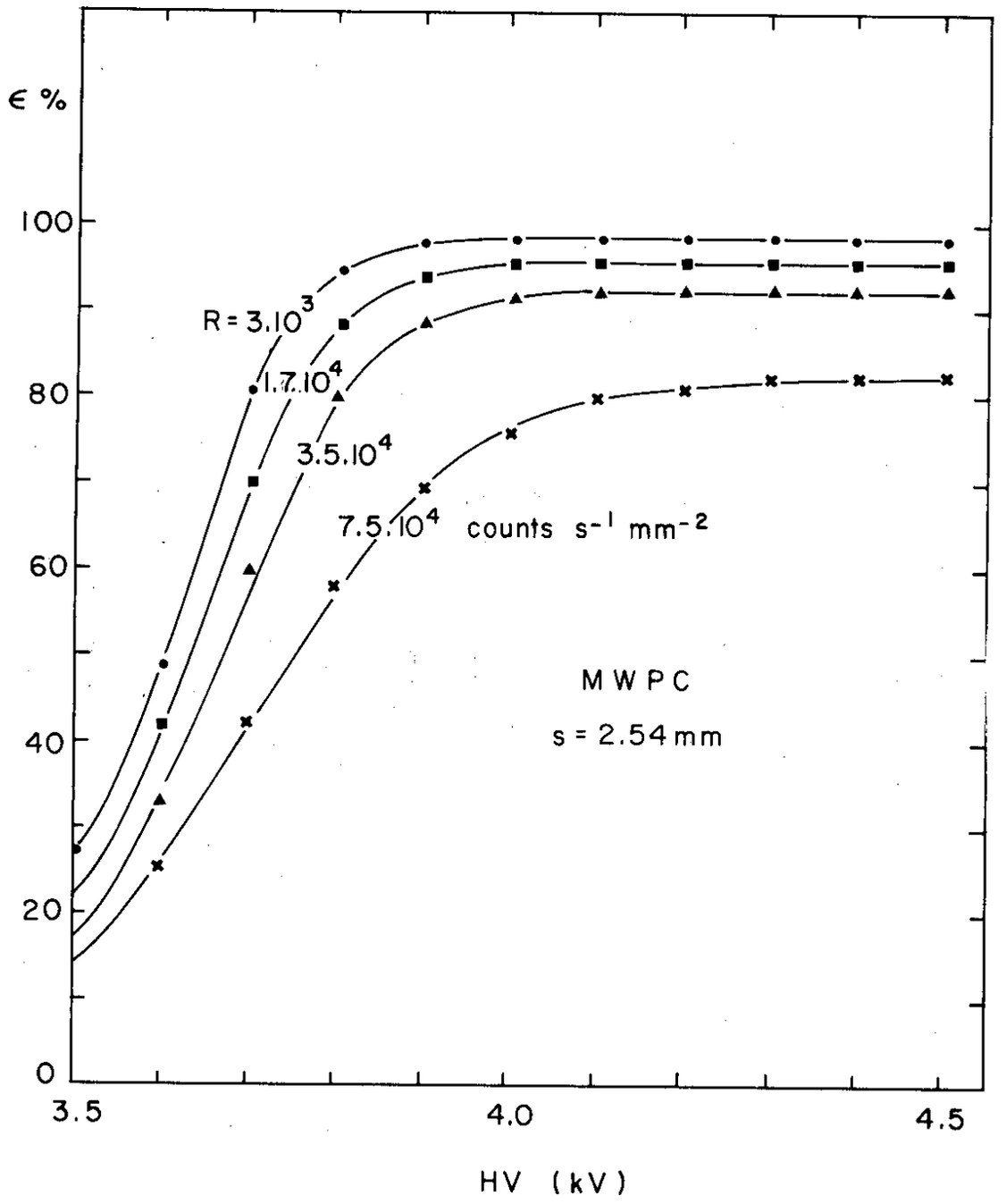
ε %
100
80
60
40
20
0
R = 3.10^3
1.7.10^4
3.5.10^4
7.5.10^4 counts s^-1 mm^-2
MWPC
s = 2.54 mm
3.5
4.0
4.5
HV (kV)

Fig. 17

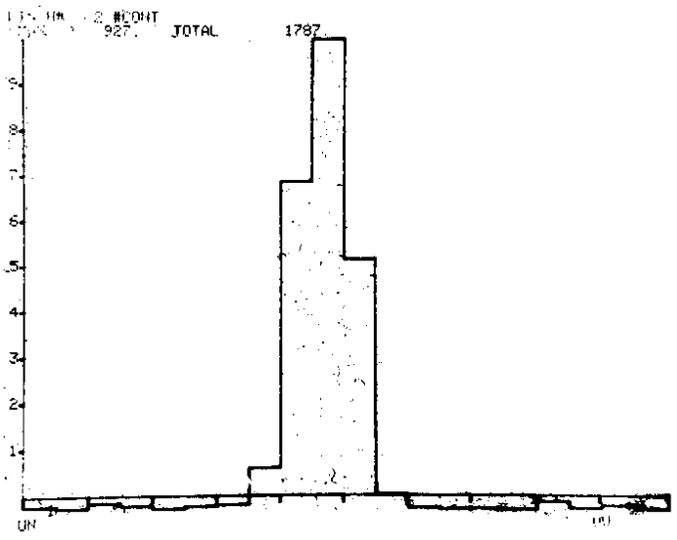

Fig. 18

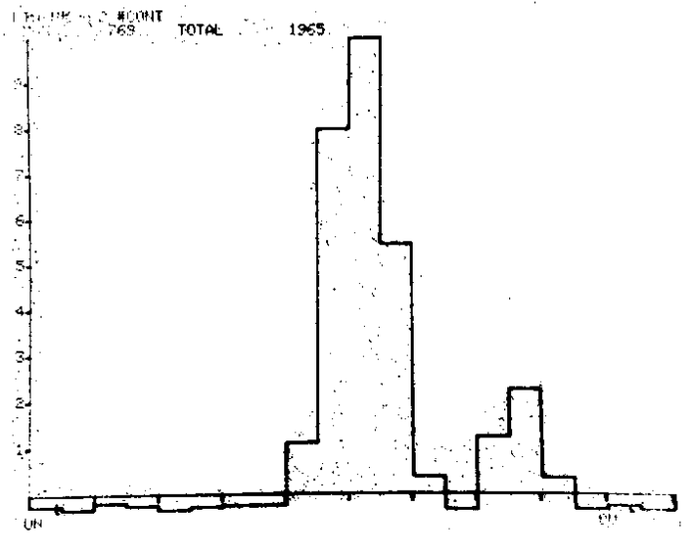

Fig. 19

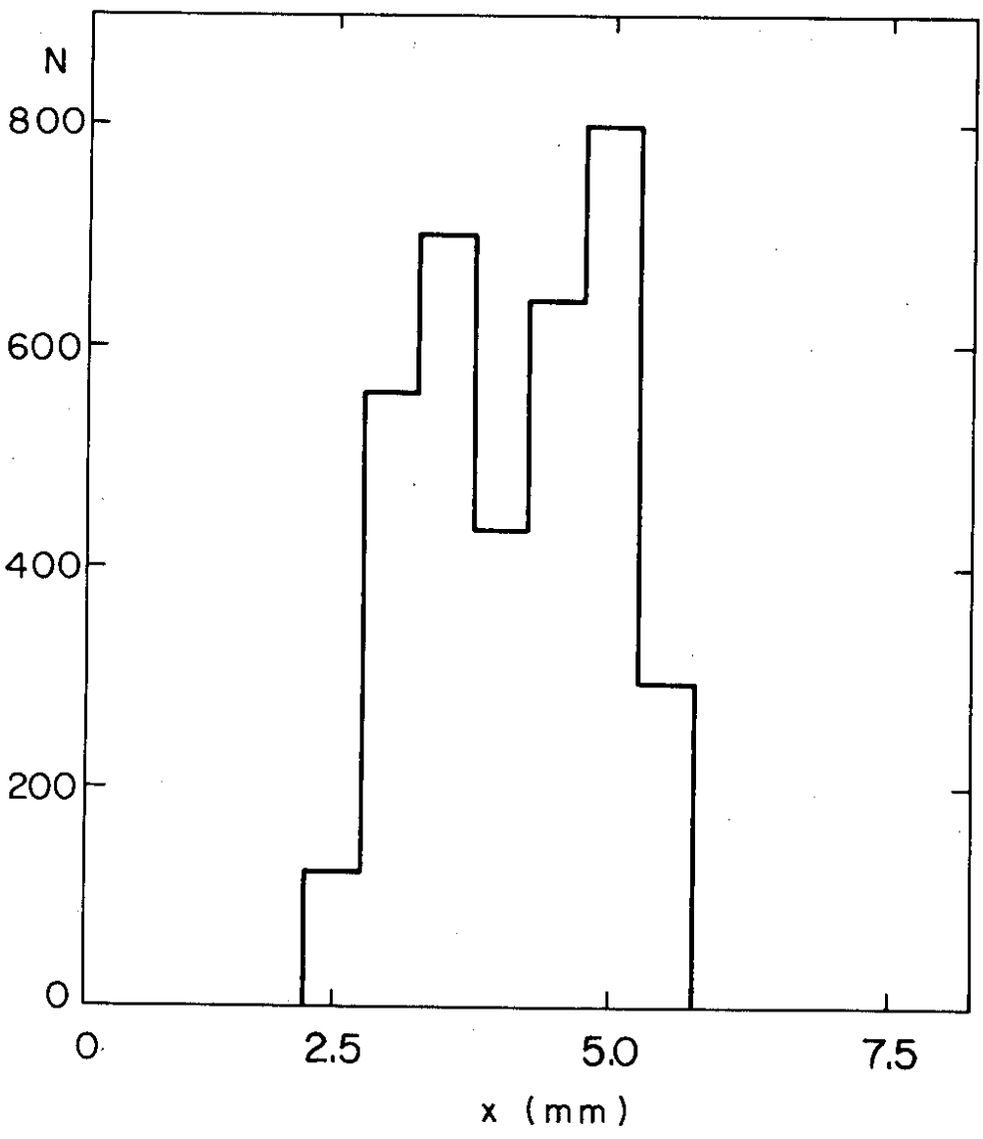

Fig. 20

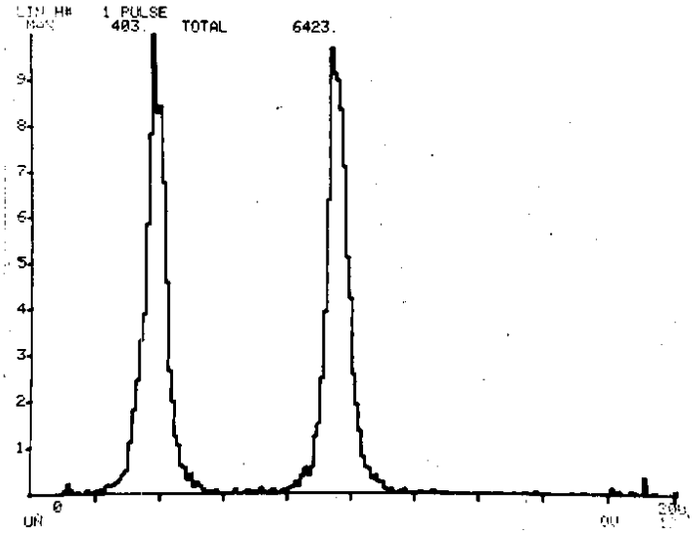

Fig. 21

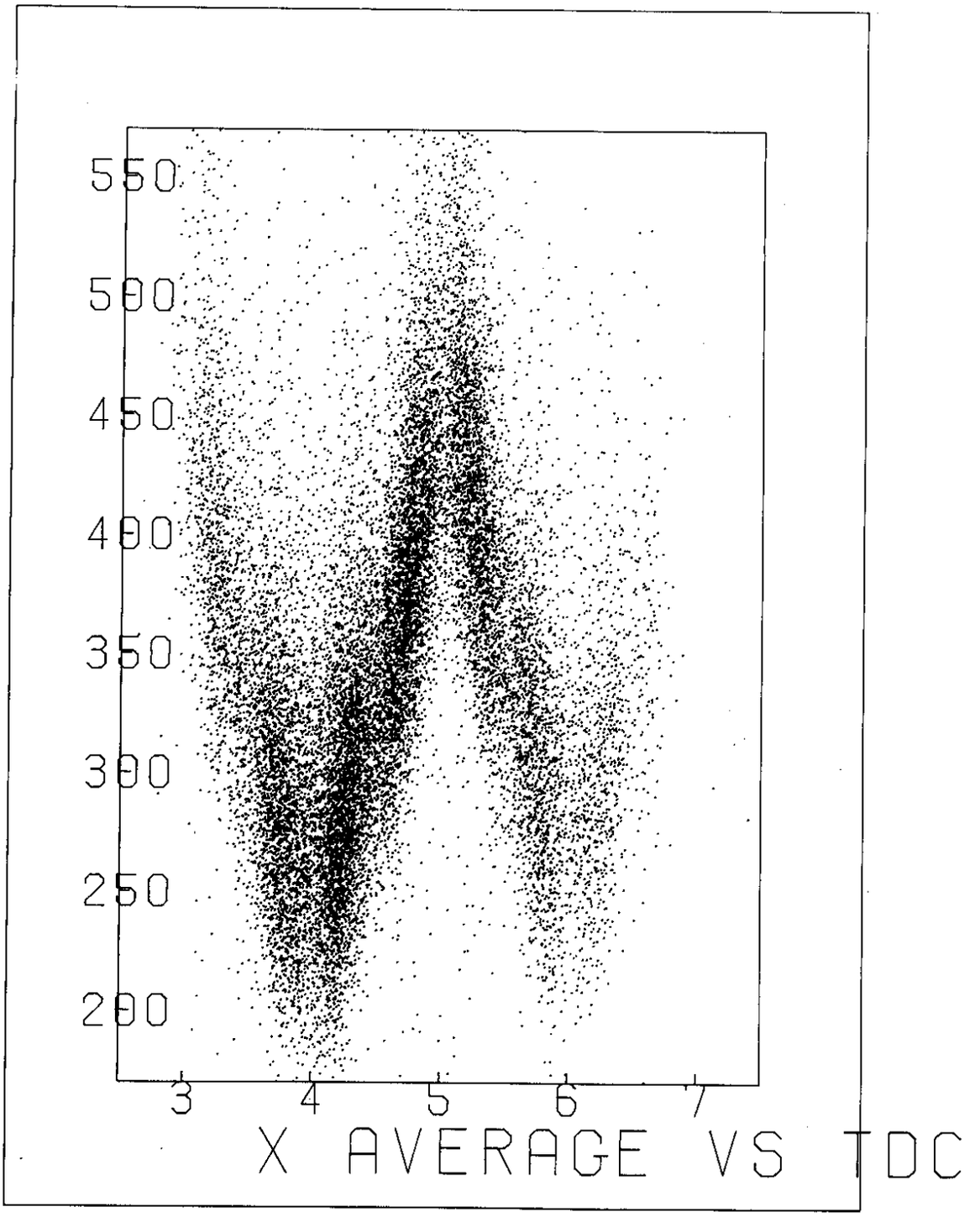

Fig. 22

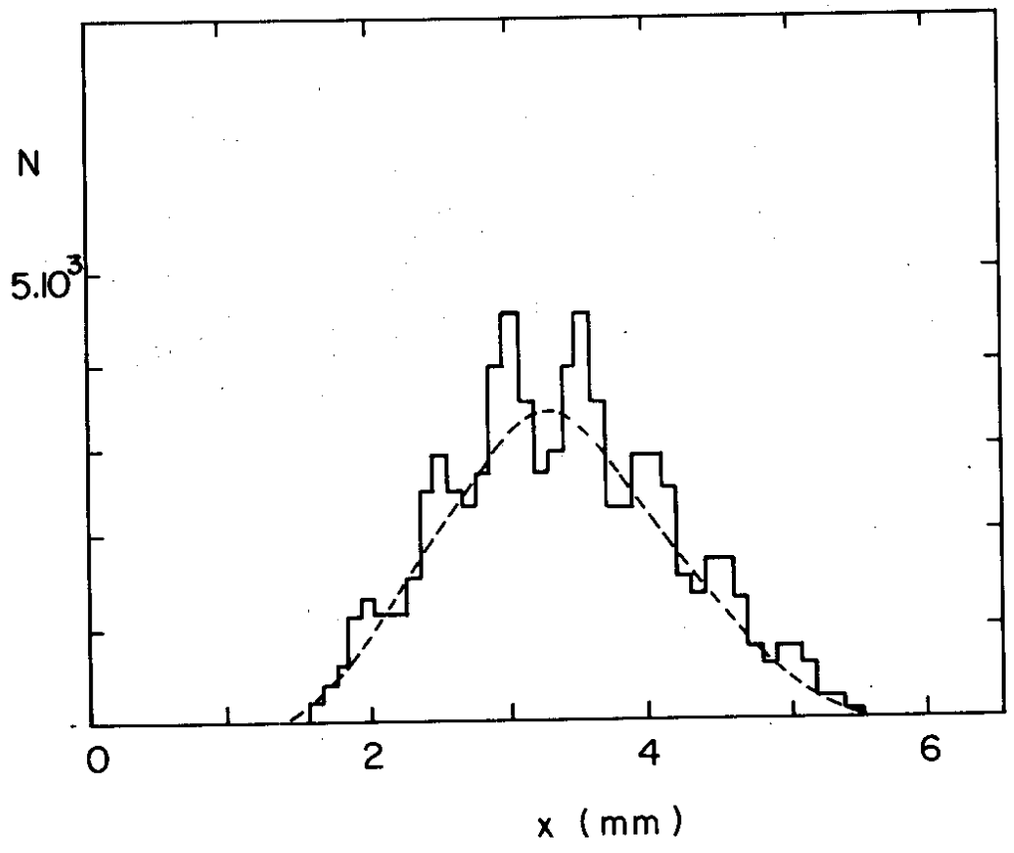

Fig. 24

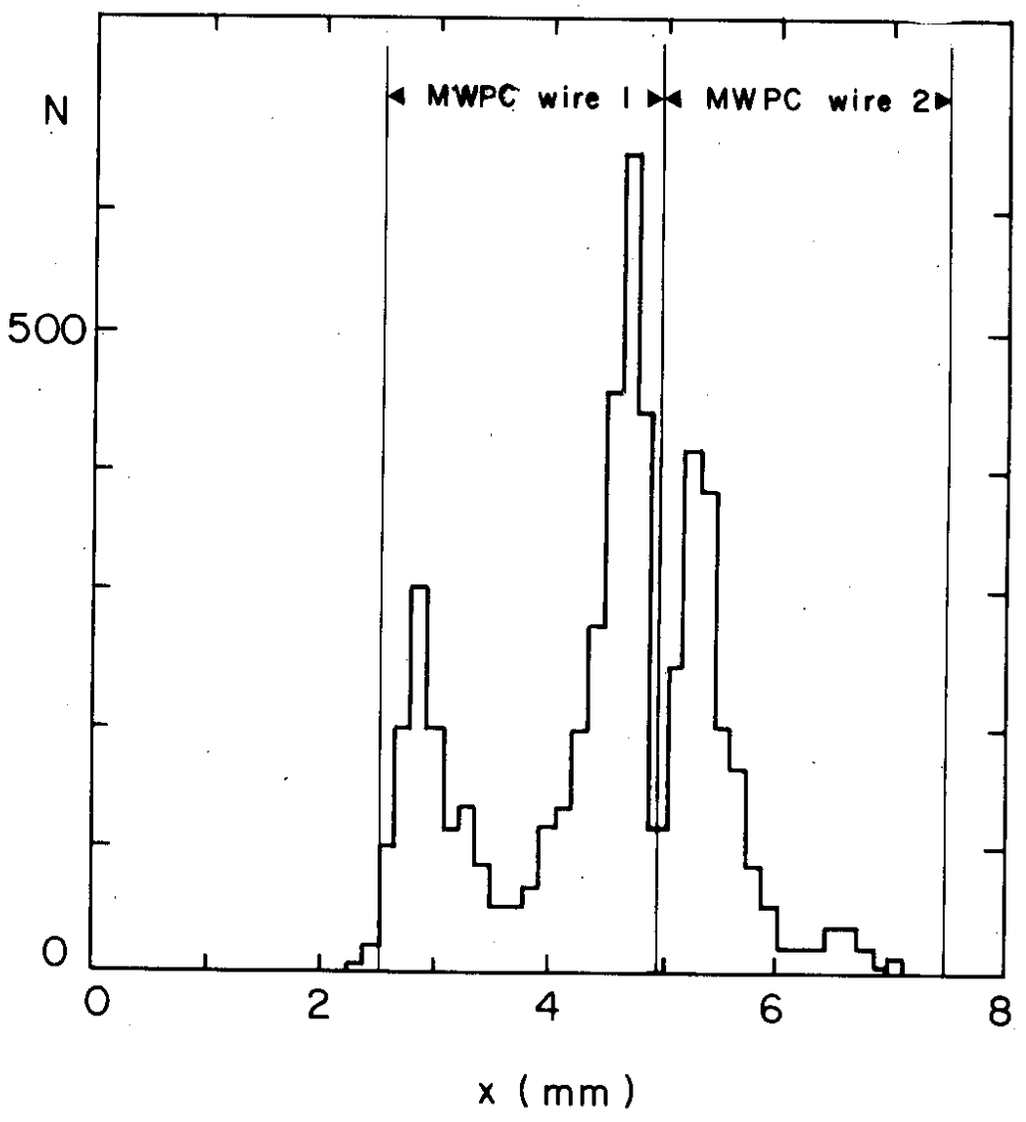

Fig. 23